

1 **Surface Ozone Distribution & Trends Over Ireland : Insights from long-**  
2 **term measurement record and source attribution modelling**

Formatted: Right: 2.54 cm, Bottom: 2.54 cm, Footer distance from edge: 1.25 cm

3  
4 Nikhil Korhale <sup>1</sup>, Tabish Ansari <sup>2</sup>, Tim Butler <sup>2</sup>, Jurgita Ovadnevaite <sup>1</sup>, [Emmanuel Chevassus](#) <sup>1</sup>,  
5 [Darius Ceburnis](#) <sup>1</sup>, [Damien Martin](#) <sup>1</sup>, Colin D.O'Dowd <sup>1</sup>, Liz

6 Coleman <sup>1</sup>

7 <sup>1</sup> School of Natural Sciences, Physics, Ryan Institute's Centre for Climate & Air Pollution  
8 Studies, University of Galway, Galway, Ireland

9 <sup>2</sup> Research Institute for Sustainability - Helmholtz Centre Potsdam, Potsdam, 14467,  
10 Germany

11  
12 **Corresponding author :**

13 Name - Dr. Liz Coleman

14 Email Id – [liz.coleman@universityofgalway.ie](mailto:liz.coleman@universityofgalway.ie)

Deleted: ¶

Formatted: Justified, Indent: Left: -0.02 cm, Hanging: 0.02 cm, Right: 0.36 cm, Space After: 13.8 pt

15 **Abstract**

16 [We present an analysis of long-term trends in surface ozone \(O<sub>3</sub>\) across Ireland, with specific](#)  
17 [focus on the Mace Head atmospheric research station, representative of Northern hemispheric](#)  
18 [background atmospheric conditions. Surface O<sub>3</sub> dataset was characterised using advanced](#)  
19 [trajectory analysis and seasonal decomposition, revealing distinct seasonal and spatial patterns.](#)  
20 [Findings show a significant rising trend in surface O<sub>3</sub> at Irish urban sites over the past two](#)  
21 [decades but without a similar trend at coastal sites. Highest O<sub>3</sub> levels and exceedances were](#)  
22 [observed at remote coastal sites, which are less susceptible to influence from local and easterly](#)  
23 [emissions but heavily influenced by transboundary pollution and stratospheric intrusion.](#)

Deleted: Surface

Deleted: pollution

Deleted: is assessed

Deleted: a

Deleted: on long-term trends with a specific focus on

30 [At Mace Head, springtime O<sub>3</sub> levels exhibit a declining trend, whereas wintertime levels show](#)  
31 [a rising trend. Focussing on the clean sector, the springtime decline remains significant, but](#)  
32 [without corresponding clean sector rising wintertime trends, implying the rising winter trends](#)  
33 [occur in response to declining local, United Kingdom \(UK\) and European emissions. Advanced](#)  
34 [modelling tools are used to quantify O<sub>3</sub> source contributions, elucidating key drivers behind](#)  
35 [the observed changes. Characteristic springtime O<sub>3</sub> maxima at Mace Head are predominantly](#)  
36 [attributed to stratospheric transport, hemispheric and long-range transport and lightning NO<sub>x</sub>.](#)  
37 [The complementary trend and sectoral observational analysis reveal a decline in total spring-](#)  
38 [time concentrations, with a more rapid decline in exceedances from the UK & continental](#)  
39 [sector.](#)

40 [This research highlights the importance of seasonal factors in air quality management across](#)  
41 [Ireland, emphasising the need for a multi-faceted approach to control O<sub>3</sub> levels and reduce](#)  
42 [exceedances through global and regional emission reductions.](#)

43 **Keywords** - Meteorology, NO<sub>x</sub>, Climate, CH<sub>4</sub>, Emissions, VOC.

#### 44 1. Introduction

45 Surface Ozone (O<sub>3</sub>) has significant implications for health, vegetation, and climate. [Its](#)  
46 [chemical production is driven by complex photochemical processes, responding non-linearly](#)  
47 [to pollution control, creating challenges for its effective regulation. Elevated O<sub>3</sub> levels cause](#)  
48 [severe health issues with, prolonged exposure to high O<sub>3</sub> levels, causing respiratory issues,](#)  
49 [cardiovascular problems, and reduced lung function, particularly in sensitive populations](#)  
50 [such as children, the elderly, and individuals with pre-existing respiratory conditions \(Lin et](#)  
51 [al., 2018; Todorović et al., 2019; Zhang et al., 2019, WHO, 2021\). O<sub>3</sub> pollution can adversely](#)  
52 [impact vegetation by reducing agricultural productivity \(Ashmore et al., 2005; Paoletti et al.,](#)  
53 [2006\). O<sub>3</sub> is also the third most significant greenhouse gas after Carbon Dioxide \(CO<sub>2</sub>\) and](#)

**Deleted:** which monitors background O<sub>3</sub> advected into Europe via prevailing South Westerlies. Using innovative trajectory analysis, O<sub>3</sub> concentrations, exceedances and were identified by sectors, revealing distinct seasonal and spatial patterns. Findings show a significant rising trend in surface O<sub>3</sub> at Irish urban sites over the past two decades but without a similar trend at coastal sites. Highest O<sub>3</sub> levels and exceedances were observed at remote coastal sites, less influenced by local emissions, and heavily influenced by meteorological processes, including transboundary pollution and stratospheric intrusion. At Mace Head, springtime O<sub>3</sub> levels show a declining trend, with a rising winter-time trend. Looking only at the clean sector, the springtime decline remains significant; but without rising wintertime trends, implying the rising winter trends are a response to declining European emissions. Advanced modelling tools are used to quantify O<sub>3</sub> source contributions, elucidating key drivers behind the observed changes. Characteristic springtime O<sub>3</sub> maxima at Mace Head are attributed to stratospheric transport, influences from westerly transboundary air pollution, and lightning NO<sub>x</sub>. Combined trend and sectoral observational analysis reveals that total spring-time concentrations are in decline, with exceedances from the UK & continental sector declining at a greater rate.

**Deleted:** As O<sub>3</sub> is highly reactive, i

**Deleted:** ,

**Deleted:** is linked to

81 methane(CH<sub>4</sub>), contributing to climate instability (IPCC, 2021). O<sub>3</sub> can live for several weeks  
82 in the free troposphere, and it is affected by large-scale atmospheric circulation patterns  
83 (Wespes et al., 2017). Meteorological factors such as temperature, solar radiation, wind  
84 speed, and atmospheric stability play a significant role in O<sub>3</sub> formation. (Ding et al., 2023;  
85 Khiem et al., 2010).

- Deleted:
- Deleted: The lifetime of
- Deleted: is on the order of several weeks,
- Deleted:
- Deleted:
- Deleted: , and m

86 O<sub>3</sub> is formed in the atmosphere from precursors Nitrogen Oxides (NO<sub>x</sub>), carbon monoxide  
87 (CO), and volatile organic compounds (VOCs) through photochemical reactions.  
88 Photochemical production requires solar radiation, and reaction rates are correlated with  
89 temperature, it is noted that little photochemical production occurs at temperatures below  
90 20°C (Coates et al., 2016). The reactive, interdependent atmospheric chemistry leads to a  
91 non-linear relationship between O<sub>3</sub> and its precursors (Seinfeld and Pandis, 2016), and  
92 effective O<sub>3</sub> mitigation requires an understanding of processes influencing O<sub>3</sub> production and  
93 removal mechanisms (Fowler et al., 2013).

- Deleted:

94 NO<sub>x</sub> can suppress or enhance O<sub>3</sub> formation, depending on local atmospheric chemistry  
95 regime. In polluted urban environments, high NO<sub>x</sub> emissions can lead to O<sub>3</sub> dissociation,  
96 retarding photochemical O<sub>3</sub> formation (NO<sub>x</sub>-saturated/VOC-limited regime), with local  
97 pollution events potentially titrating surface O<sub>3</sub> completely, converting NO to NO<sub>2</sub>. This  
98 effect is more prevalent in wintertime, when temperatures are low, and there is little solar  
99 radiation to facilitate photochemical production of O<sub>3</sub>. In relatively clean environments, O<sub>3</sub>  
100 formation is correlated with NO<sub>x</sub> concentration (Tavella & da Silva Júnior, 2021).

- Deleted: the

- Deleted: retarding formation whereas i

- Deleted: Seinfeld and Pandis, 1997;

101 O<sub>3</sub> and precursors can be transported over great distances in the troposphere, with transport  
102 from distant polluted regions accounting for 40% of O<sub>3</sub> abundance in remote regions (Sudo and  
103 Akimoto, 2007). While O<sub>3</sub> is transported in air masses from distant sources, although titration  
104 occurs, O<sub>3</sub> is replenished via mixing. Over Ireland, advection of O<sub>3</sub> rich air from continental  
105 outflow is a significant source of Irish O<sub>3</sub>, but European continental air-masses can also

116 [transport pollutants to trigger O<sub>3</sub> depletion events, but the O<sub>3</sub> depleting effect of the air masses](#)  
117 [originating from Europe is in decline in response to European Union \(EU\) pollution control](#)  
118 [strategies \(Derwent et al., 2024\).](#)

119 Seasonal and regional variations further complicate the regulation, with higher O<sub>3</sub> levels  
120 observed in summer across the northern hemisphere due to increased temperatures, solar  
121 radiation, and abundant precursors (Moiseenko et al., 2021; Sicard et al., 2016). In marine  
122 boundary layers, O<sub>3</sub> levels are generally lower than in continental regions, though specific  
123 oceanic environments can exhibit high O<sub>3</sub> concentrations due to inflows from polluted areas  
124 (Boylan et al., 2014; Girach et al., 2020). [Another factor which influences O<sub>3</sub> levels is the](#)  
125 [North Atlantic Oscillation \(NAO\), which influences O<sub>3</sub> levels in Western Europe. During a](#)  
126 [positive NAO phase, O<sub>3</sub> levels increase. In contrast, during a negative NAO phase \(NAO-](#)  
127 [low\), O<sub>3</sub> levels decrease. This effect is particularly notable in southwest, central, and northern](#)  
128 [Europe \(Bonaccorso et al., 2015; Creilson et al., 2003; Pausata et al., 2012\).](#)

129 While Ireland's air quality is mostly governed by the influx of clean maritime air from the  
130 Atlantic Ocean (Tripathi et al., 2010), [certain](#) synoptic scenarios allow for the intrusion of  
131 polluted air masses from continental Europe. These events, though infrequent, can bring  
132 substantial amounts of [O<sub>3</sub>](#) and its precursors (NO<sub>x</sub> and VOCs), contributing to short-term O<sub>3</sub>  
133 pollution episodes.

134 The World Health Organisation (WHO) publishes Air Quality Guidelines (AQGs) as a non-  
135 legally binding global target for governments to achieve within their jurisdictions. These  
136 AQGs comprise evidence-based recommendations of limit values to protect public health.  
137 The current recommended AQGs for O<sub>3</sub> is expressed as a daily maximum of 8-hourly running  
138 average O<sub>3</sub> value of 100 µg/m<sup>3</sup>. Days when O<sub>3</sub> levels exceed the recommended AQGs are  
139 classified as exceedance days. Factors contributing to exceedances include high solar  
140 radiation, stagnant air masses, and local emissions and regional and transboundary transport

**Deleted:** Another factor which influences O<sub>3</sub> level is the North Atlantic Oscillation (NAO) which influences O<sub>3</sub> levels in Western Europe, with positive phases enhancing the transport of O<sub>3</sub> and precursors from North America. This effect is particularly notable in southwest, central, and northern Europe (Bonaccorso et al., 2015; Creilson et al., 2003; Pausata et al., 2012)....

**Deleted:** particular

**Deleted:** ozone

**Deleted:** ,

151 of O<sub>3</sub> and precursors. Globally, over the past 150 years, there has been a 40% increase in O<sub>3</sub>  
152 levels owing to rising precursor emissions. (Archibald et al., 2020; Griffiths et al., 2021;  
153 Young et al., 2013). Despite European Union emission reduction policies, O<sub>3</sub> pollution  
154 remains a problem, with over 94% of those living in European cities exposed to O<sub>3</sub> levels  
155 exceeding the WHO AQGs in 2022 (EEA 2024, WHO 2021). Over 22,000 premature deaths  
156 in the EU were attributable to short-term exposure to O<sub>3</sub> in 2021 (Soares et al., 2023).

Deleted: Over

157 Long-term O<sub>3</sub> measurement data from the Mace Head research station in Ireland reveal a  
158 distinct seasonal pattern with peaks during spring and lows in summer. (Derwent, 1998;  
159 Derwent et al., 1994, 2018). Historical trends show increasing baseline O<sub>3</sub> levels in the 1980s  
160 and 1990s, stability in the 2000s, and a decline in the 2010s (Derwent et al., 2013; Derwent  
161 et al., 2018). Recent observational and modelling data have identified a broad O<sub>3</sub> maximum  
162 in spring and early summer, aligning with peak stratospheric transport (Ansari et al., 2024;  
163 Lin et al., 2012; Russo et al., 2023). O<sub>3</sub> dynamics are complex, and studies reveal  
164 discrepancies between model output and observations (Bessagnet et al., 2016; Vautard et al.,  
165 2012), highlighting the need for further understanding of factors governing O<sub>3</sub> levels and  
166 trends.

Deleted: in O<sub>3</sub>

Deleted: a

Deleted: .

Deleted: , Manning, Simmonds, Spain,

167 This study investigates the distribution and trends of O<sub>3</sub> and its precursors across Ireland,  
168 providing valuable insights into the regional and hemispheric impact on Irish surface O<sub>3</sub> levels

169 and exceedances. We analyse the long-term O<sub>3</sub> observational dataset for Ireland, identifying the  
170 mean and range of O<sub>3</sub> levels and seasonal variation at each site. We identify the long-term  
171 annual and monthly trends at each site, quantifying the significance of each trend according to  
172 TOAR guidelines (Chang et al., 2023). We also identify the frequency and seasonality of  
173 exceedance of the WHO AQGs for the protection of human health from O<sub>3</sub> pollution for each  
174 site. The trends and seasonality are contextualised by looking at trends in the Irish instrumental  
175 record of dominant precursors of NO<sub>x</sub> and CH<sub>4</sub> and we discuss the relationship between NO<sub>x</sub>

Deleted: By analysing

Deleted: a

Deleted: long

184 [and O<sub>3</sub> by comparing anomalies between monthly average NO<sub>x</sub> and O<sub>3</sub> during lockdown](#)  
185 [compared to the average values for the three years prior to lockdown.](#) Advanced modelling  
186 results using the Tropospheric Ozone Attribution of Sources with Tagging 1.0 (TOAST 1.0)  
187 framework (Butler et al., 2018; Butler et al., 2020) [are validated against measurements at various](#)  
188 [sites for simulation period 2000-2018, and the simulation results analysed to determine the](#)  
189 [geographical and sectoral source of precursors that contribute to simulated O<sub>3</sub> at Mace Head,](#)  
190 [identifying seasonality and long-term trends in the sources. Finally, the observational data are](#)  
191 [classified using advanced trajectory clustering methods to separate air masses from the clean](#)  
192 [sector from those influenced by local, UK or EU emission sources, with seasonal trends](#)  
193 [identified for both clean and polluted sectors, and the exceedances classified as coming from](#)  
194 [either the clean or polluted sector.](#)  
195 [This research highlights significant seasonal and temporal variations and long-term trends in](#)  
196 [O<sub>3</sub> concentrations, and the integrated approach, including observational and modelling](#)  
197 [analysis, enhances our understanding of the drivers of O<sub>3</sub> concentrations, trends and](#)  
198 [exceedances over Ireland and allows quantification of global and regional contributions to Irish](#)  
199 [surface O<sub>3</sub>.](#)

**Deleted:** , this research highlights significant seasonal and temporal variations and long-term trends in O<sub>3</sub> concentrations.

## 201 **2. Data and methodology**

### 202 **2.1 Observational Network and Analysis Approach**

203 Measurement data is obtained from the Environmental Protection Agency, Ireland (EPA)  
204 (<https://eparesearch.epa.ie/safer/>). The O<sub>3</sub> monitoring network shown in Figure 1 has been  
205 operational in Ireland since 1994. O<sub>3</sub> is measured using an API M400 and O<sub>3</sub> analyser based  
206 on UV photometry at all monitoring sites. [At the Mace Head site, O<sub>3</sub> was measured using a](#)  
207 [Monitor Labs 8810 analyzer and a Thermo Environmental O<sub>3</sub> monitor. Measurement operating](#)

**Deleted:** were applied to determine the drivers of O<sub>3</sub> trends in Ireland. Additionally, trajectory analysis is used to trace the origins of air masses, revealing the impact of transboundary pollution and atmospheric transport. This integrated approach not only enhances our understanding of the drivers of O<sub>3</sub> concentrations, trends and exceedances over Ireland but also underscores the importance of global and regional contributions to O<sub>3</sub>.

**Formatted:** Indent: Left: 0 cm, Right: 0 cm, Space After: 0 pt

219 accuracy is within 1.0 ppb, based on precision, calibration and drift characteristics,

220 Measurements of O<sub>3</sub> precursors from EPA air quality monitoring sites are also monitored. The

221 details of the measurements sites are shown in Table 1. Numerous previous studies have

222 analysed this data, with a particular focus on the analysis of Mace Head data to assess

223 background O<sub>3</sub> (Carslaw, 2005; Derwent, 1998; Derwent et al., 1994, 1998, 2001, 2004, 2008,

224 2013; Derwent, Manning, Simmonds, & Doherty, 2018; Derwent, Manning, Simmonds, Spain,

225 et al., 2018; Oltmans et al., 2013; Simmonds et al., 2004; Tripathi et al., 2010, 2012, 2013).

226 CH<sub>4</sub> data is obtained from the Integrated Carbon Observation System (ICOS) network,

227 accessible at [https://www.icoscp.eu/data-products/ATM\\_NRT\\_CO2\\_CH4](https://www.icoscp.eu/data-products/ATM_NRT_CO2_CH4).

228 For this analysis, the observational sites were classified into three categories: Coastal, Rural,

229 and Urban, as shown in Figure 1. The classification of the sites is based on Spohn et al., 2022,

230 with the addition of the coastal category. Hourly data were used to evaluate annual trends

231 based on monthly mean concentrations. Seasonal analysis conducted for the four main

232 meteorological seasons in Ireland, namely Spring (March, April, May), Summer (June, July,

233 August), Autumn (September, October, November), and Winter (December, January,

234 February). O<sub>3</sub> exceedances were calculated based on the WHO AQGs, indicating that the

235 maximum daily average over eight hours (MDA8) should not exceed 100 µg/m<sup>3</sup>. A

236 significant analysis was performed on data measured at the Mace Head Atmospheric

237 Research Station (53°33'N, 9°54' W), which is exposed to pristine marine air masses

238 approximately half of the time. (Grigas et al., 2017; O'Dowd et al., 2014).

239 **Table 1.** Details of Environmental Protection Agency Ireland (EPA) O<sub>3</sub> measurement sites  
240 over Ireland, with location information, and the data period used for the study.

241

242

243

Deleted: .

Deleted: table

Deleted:

Deleted: ¶

Deleted: ¶

Deleted: levels of

Deleted: ¶

Formatted: Subscript

Deleted: ¶  
O. P.

Deleted: n.d.,

Deleted:

Deleted:

Deleted: Additionally, the

Formatted: Space After: 12.6 pt

Deleted: ¶

Deleted: Site

... [1]

259

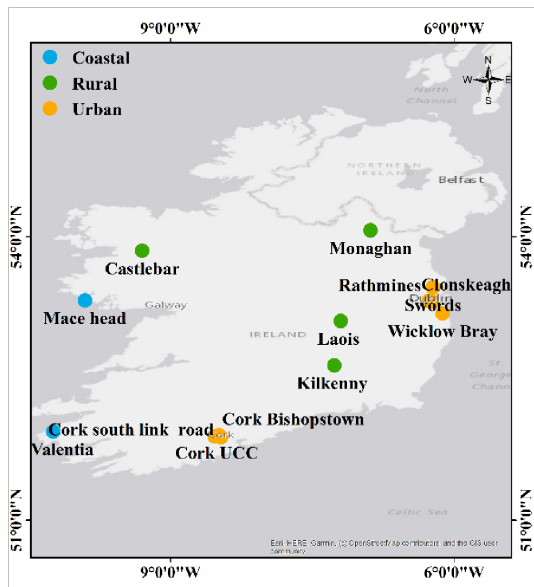
Site	Data availability	Type	Latitude	Longitude
<a href="#">Mace head</a>	<a href="#">1994-2022</a>	Coastal	<a href="#">53.3253</a>	<a href="#">-9.9036</a>
<a href="#">Valentia</a>	<a href="#">2001-2022</a>	Coastal	<a href="#">51.9385</a>	<a href="#">-10.24</a>
<a href="#">Monaghan</a>	<a href="#">1995-2022</a>	Rural	<a href="#">54.0661</a>	<a href="#">-6.883</a>
<a href="#">Laois</a>	<a href="#">2005-2022</a>	Rural	<a href="#">53.1076</a>	<a href="#">-7.1983</a>
<a href="#">Kilkenny</a>	<a href="#">2012-2022</a>	Rural	<a href="#">52.6383</a>	<a href="#">-7.2676</a>
<a href="#">Castlebar</a>	<a href="#">2009-2022</a>	Rural	<a href="#">53.851</a>	<a href="#">-9.3003</a>
<a href="#">Rathmines</a>	<a href="#">2002-2022</a>	Urban	<a href="#">53.322</a>	<a href="#">-6.2672</a>
<a href="#">Clonskeagh</a>	<a href="#">2008-2022</a>	Urban	<a href="#">53.3118</a>	<a href="#">-6.2353</a>
<a href="#">Swords</a>	<a href="#">2009-2022</a>	Urban	<a href="#">53.4631</a>	<a href="#">-6.2222</a>
<a href="#">Wicklow Bray</a>	<a href="#">2009-2022</a>	Urban	<a href="#">53.1873</a>	<a href="#">-6.122</a>
<a href="#">Cork South link road</a>	<a href="#">2014-2022</a>	Urban	<a href="#">51.8785</a>	<a href="#">-8.4649</a>
<a href="#">Cork Bishops town</a>	<a href="#">2016-2022</a>	Urban	<a href="#">51.8858</a>	<a href="#">-8.53321</a>
<a href="#">Cork UCC</a>	<a href="#">2018-2022</a>	Urban	<a href="#">51.9</a>	<a href="#">-8.4863</a>

260

261

262

263 **Figure 1.** – The map of EPA O<sub>3</sub> measurement sites over Ireland with classification of  
 264 backgrounds.



265 Trend analysis was conducted using the Openair package in R, software designed for the  
266 analysis of atmospheric composition data. Trends were determined using the Theil-Sen slope  
267 estimator and Mann-Kendall tests to quantify significance, in accordance with the  
268 Tropospheric Ozone Assessment Report (TOAR) guidelines (Lefohn et al., 2018). [Theil-Sen](#)  
269 [directly provides a robust slope estimate. It is a reliable measure of change over time for](#)  
270 [direct interpretation and comparison. It is a robust method for estimating trend slopes in time](#)  
271 [series data, preferable to traditional least-squares regression, which can be sensitive to](#)  
272 [extreme values and outliers.](#) Uncertainty or reliability of the trend is calibrated according to  
273 the p-value, as outlined by (Chang et al., 2023), consistent with the best statistical practices  
274 for analysis used in the second phase of TOAR.

Deleted: .

Deleted: This

Deleted: tool is

Deleted:

Deleted: It is a robust method for estimating trend slopes in time series data, preferable to traditional least-squares regression, which can be sensitive to extreme values and outliers.

## 275 2.2 Clean air sector identification from Back trajectories

276 Baseline O<sub>3</sub> refers to the concentration of O<sub>3</sub> in air masses minimally influenced by local or  
277 regional anthropogenic emissions. Back-trajectory methods are widely used to estimate  
278 baseline O<sub>3</sub> levels by analysing the origins and transport pathways of air masses reaching  
279 observation sites. Typically, Lagrangian dispersion models are used to trace air parcels  
280 backwards in time and identify their origin.

Formatted: Indent: Left: 0 cm, Right: 0 cm

281 For this study, air mass trajectories arriving at Mace Head were calculated using the Hybrid  
282 Single Particle Lagrangian Integrated Trajectory Model (HYSPPLIT) (Draxler et al., 2003; Stein  
283 et al., 2015) in conjunction with R software. The air masses were classified into two categories:  
284 the clean sector and EU-influenced sector. An air mass was considered part of the clean sector  
285 when air mass trajectories remained over the ocean surface for the previous 72 hours, the  
286 remaining air mass trajectories are classified as the EU-influenced sector. Meteorological data  
287 for the analysis were derived from NOAA reanalysis data (Stunder et al., 2004). [The 72h](#)  
288 [duration captures regional/long-range transport without trajectory error from meteorological](#)  
289 [uncertainties. The 100 m height was used to represent the well-mixed flow of the boundary](#)

Formatted: Justified, Indent: Left: 0 cm, Hanging: 0.02 cm, Space After: 0 pt, Line spacing: Multiple 1.99 li

Deleted: consider

Deleted: s. ¶  
And

Deleted: ¶

Deleted: ¶

303 [layer above the surface. The 06:00 UTC aligns with synoptic times and can match daily O<sub>3</sub>](#)  
304 [cycles or measurement periods. Therefore,](#) calculations were performed for 6:00 UTC each  
305 day, with a final trajectory height of 100 meters, covering the years 2000 to 2022. The O<sub>3</sub>  
306 concentrations observed during the clean sector were averaged to derive baseline levels,  
307 consistent with previous studies on baseline O<sub>3</sub> trends and sources (Derwent et al., 2013;  
308 Oltmans et al., 2006).

Deleted: C

### 309 2.3 CAM4-Chem Model

310 The CAM-Chem air quality model, part of the Community Earth System Model (CESM),  
311 simulates atmospheric chemistry and the interactions among chemical constituents,  
312 meteorology, and climate. It incorporates detailed chemical mechanisms, emission inventories,  
313 and meteorological data to simulate pollutant dispersion, thereby allowing us to determine air  
314 quality trends. CAM-Chem has been applied in numerous studies, significantly contributing to  
315 the understanding of regional and global atmospheric processes. (Lamarque et al., 2012; Tilmes  
316 et al., 2016). The model features a flexible chemical pre-processor to allow for detailed  
317 handling of atmospheric chemistry. Studies have demonstrated that CAM-Chem accurately  
318 represents conditions in both the troposphere. (Aghedo et al., 2011; Lamarque et al., 2010) and  
319 the stratosphere (Lamarque et al., 2008; Lamarque and Solomon, 2010), including temperature  
320 structure and dynamics (Butchart et al., 2011). Offline CAM-Chem has also been utilised in  
321 the Hemispheric Transport of Air Pollution (HTAP) assessments. (Anenberg et al., 2009; Fiore  
322 et al., 2009; Jonson et al., 2010; Shindell et al., 2008; Tan et al., 2018).

Deleted: ¶

Formatted: Indent: Left: 0 cm, Right: 0 cm

323 For the current study, we analyse simulations of the Community Atmospheric Model version 4  
324 CAM4-Chem (Community Atmosphere Model version 4 with chemistry) ((Lamarque et al.,  
325 2012). [The model simulations were carried out at a horizontal resolution of 210 km × 280 km,](#)  
326 [with 56 vertical levels for the 2000-2018 period,](#) with specified dynamics derived from  
327 MERRA2 reanalysis. (Molod et al., 2015). [The coarse spatial resolution, it is still appropriate](#)

Deleted: The model simulations were carried out at a horizontal resolution of 1.9° × 2.5°, featuring 56 vertical levels for the 2000-2018 period,

334 [because it provides a reliable representation of the regional background atmosphere](#)  
335 [influencing the urban sites. The model captures large-scale features of atmospheric transport,](#)  
336 [seasonal variability, and background O<sub>3</sub> levels, all of which are essential for interpreting urban](#)  
337 [observations. Comparing urban measurements with regional-scale CAM-Chem outputs allows](#)  
338 [local pollution effects to be distinguished from regional atmospheric influences.](#)

339 Tagged source attribution of tropospheric ozone (TOAST 1.0) is a novel tagging methodology  
340 developed for the CESM to quantify source contributions to O<sub>3</sub>. Unlike traditional methods  
341 that rely on sensitivity simulations, TOAST uses an online tagging approach to track O<sub>3</sub>  
342 production from specific NO<sub>x</sub> and VOC sources (e.g., anthropogenic, biogenic, biomass  
343 burning, lightning) directly within the model, allowing for efficient attribution of O<sub>3</sub> to regional  
344 and sectoral emissions while maintaining full chemical coupling. The tool has been validated  
345 against observations and demonstrates utility in disentangling the impacts of different emission  
346 sectors on O<sub>3</sub> pollution. (Butler et al., 2018, 2020; Lupaşcu et al., 2022; Nalam et al., 2024).

347 [The model results have inherent standard uncertainties common in any modelling exercise, i.e.,](#)  
348 [uncertainties in emission inventories in terms of magnitude and spatial accuracy; uncertainties](#)  
349 [in model parameters, e.g., surface resistance for deposition for various surfaces, boundary layer](#)  
350 [mixing, photolysis, chemical kinetic parameters \(Wild et al., 2025\) and structural deficiencies](#)  
351 [such as a coarse resolution and missing processes \(e.g., halogen chemistry; Saiz-Lopez et al.,](#)  
352 [2025\). The sum of all tagged contributions very closely matches the total simulated ozone](#)  
353 [\(which is simulated independently and is not just an algebraic sum of the tagged contributions\)](#)  
354 [is a good validation of the tagging mechanism \(Butler et al., 2018 and 2020\).](#)

355 Global CAM4-Chem model simulations are performed for the years 2000-2018 with NO<sub>x</sub> and  
356 VOC tagging (as described in Ansari et al., 2025; Nalam et al., 2025), with the base chemical  
357 mechanism (Emmons et al., 2012) and source code modified to account for extra tagged species

Deleted:

Formatted: Indent: Left: 0.01 cm, Right: 0 cm, Line spacing: Double

Deleted: ¶

Formatted: Font colour: Text 1

Deleted: (MOZART;

361 representing regional and sectoral identities. Anthropogenic emissions of NO<sub>x</sub>, CO, and non-  
362 methane volatile organic compounds (NMVOCs) are incorporated from the Hemispheric  
363 Transport of Air Pollution version 3 emissions inventory. (HTAPv3; Crippa et al., 2024), which  
364 includes land-based emissions, international shipping emissions, and aircraft emissions.  
365 Biomass burning emissions are sourced from the GFED-v4 inventory (Van Der Werf et al.,  
366 2010), while biogenic NMVOC emissions are derived from CAM4-GLOB-BIOv3.0. The O<sub>3</sub>  
367 source attribution technique used for this study is described in (Butler et al., 2020).

368

### 369 3. Results and discussions

#### 370 3.1 Yearly variation of O<sub>3</sub>

371 Figure 2 shows box plots, illustrating the average O<sub>3</sub> concentrations for 13 sites over the  
372 duration of the available dataset, as discussed in section 2.1 providing a comprehensive  
373 overview of the variability and distribution of O<sub>3</sub> concentration. [Coastal sites, Mace Head and](#)  
374 [Valentia, show higher O<sub>3</sub> levels compared to other sites, with annual average concentrations of](#)  
375 [77 µg/m<sup>3</sup> and 69 µg/m<sup>3</sup>, respectively.](#) In urban areas like Rathmines, Dublin, O<sub>3</sub> concentrations  
376 remained consistently lower, with averages ranging from 39 to 56 µg/m<sup>3</sup>. Similarly, South link  
377 road and Bishopstown sites in Cork city, recorded relatively lower concentrations compared to  
378 coastal and rural locations, reflecting the impact of high urban NO<sub>x</sub> emissions. Rural sites like  
379 Laois and Kilkenny showed intermediate O<sub>3</sub> concentrations, less influenced by urban  
380 emissions. These sites consistently show O<sub>3</sub> averages ranging between 50 to 57 µg/m<sup>3</sup>, with  
381 little variability, highlighting the predominant role of steady background O<sub>3</sub> contributions in  
382 rural sites. O<sub>3</sub> concentrations vary significantly with proximity to emission sources – adjacent  
383 to urban areas, O<sub>3</sub> levels can be lower due to titration, where O<sub>3</sub> reacts with NO, causing O<sub>3</sub>

Formatted: Indent: Left: 0 cm, Right: 0 cm

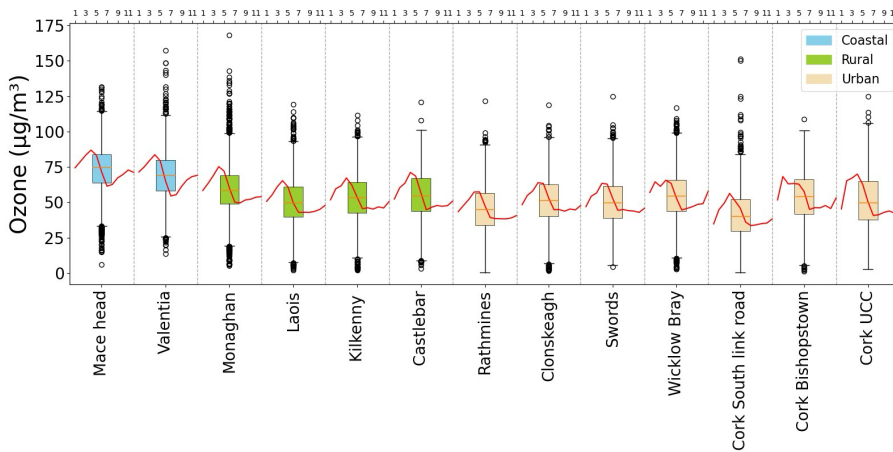
Deleted:

Deleted: Coastal sites, such as Mace Head, show higher O<sub>3</sub> levels compared to other sites, with an annual average concentration 77 µg/m<sup>3</sup>. Similarly, Valentia shows higher mean concentrations at 78 µg/m<sup>3</sup> (in 2003).

389 depletion, but the transport of precursors can cause an increase in O<sub>3</sub> concentration downwind  
 390 of the sources (Jeon et al., 2014; Monks et al., 2015;Zhu et al., 2012)

391 The red line over the box shows a clear seasonal pattern in O<sub>3</sub> concentration for each site,  
 392 with a springtime (March-April) peak and summertime (June-July), dip, with the highest  
 393 peaks in the coastal sites, and lowest dips in urban sites, influenced by local emissions e.g.  
 394 Cork South Link Road and Swords.

Deleted: . W  
 Deleted: -  
 Deleted: -



395  
 396 **Figure 2.** Annual average O<sub>3</sub> concentration at different sites in Ireland. In each box, the  
 397 lowest whisker level represents the 5<sup>th</sup> percentile, the box spans from the 25<sup>th</sup> to the 75<sup>th</sup>  
 398 percentile, the horizontal line within the box represents the median 50<sup>th</sup> percentile, and the  
 399 upper whisker represents the 95<sup>th</sup> percentile. The average of monthly O<sub>3</sub> values calculated  
 400 for the entire period of each station, and the red line shows the average monthly O<sub>3</sub> variation  
 401 of all sites top axis shows the month (1– 12).

405

## 406 3.2 O<sub>3</sub> Trend analysis

### 407 3.2.1 Yearly trend

408 Table 2. [summarises](#) the Theil-Sen trends in O<sub>3</sub> concentration (in µg/m<sup>3</sup> per year) across 13  
 409 monitoring sites in Ireland over different periods: 5 years (2018-2022), 10 years (2013-2022),  
 410 15 years (2008-2022), and the available years of data for each site. In the coastal regions,  
 411 Mace Head shows a consistent decrease in O<sub>3</sub> levels over the 5, 10, and 15-year periods,  
 412 although the entire dataset exhibits a small rising trend 0.02 µg/m<sup>3</sup> per year. These trends are  
 413 mostly in agreement with previous studies, where there was a positive trend observed in  
 414 background O<sub>3</sub> up to the mid-2000s, which stabilised and began to decline in the 2010s  
 415 (Derwent et al., 2018). Valentia shows a long-term decreasing trend of -0.23 µg/m<sup>3</sup> per year,  
 416 consistent with the previous study by Tripathi et al..2010.

417 In rural areas, Monaghan exhibits a declining trend in O<sub>3</sub> concentrations across all time  
 418 periods, indicating an overall reduction. Laois shows an upward trend over the 10 and 15-  
 419 year periods, though there is a slight decline in the most recent 5 years. Kilkenny presents  
 420 slight negative trends over the 5 and 10-year periods (-0.29 and -0.01µg/m<sup>3</sup> per year).  
 421 Negative trends are observed in Castlebar(-0.71 and -0.05 µg/m<sup>3</sup> per year).

422 The Dublin urban area sites (Rathmines, Clonskeagh, Swords) predominantly show increasing  
 423 trends in O<sub>3</sub> levels, indicative of changes in urban pollution or local emissions, with decreased  
 424 suppression of O<sub>3</sub> levels in urban regions due to decreased local emissions. (Derwent et al.,

425 2024). This is consistent with the “weekend effect,” as observed by [Atkinson-Palombo et al.](#)  
 426 [\(2006\)](#) whereby a reduction in NO<sub>x</sub> due to reduced weekend traffic decreases O<sub>3</sub> removal by  
 427 NO<sub>x</sub> titration, leading to higher surface O<sub>3</sub> levels, likely to occur in wintertime, and in regions  
 428 with low photochemical [production](#) due to low insolation [and temperatures](#), as [observed in](#)

Formatted: Indent: Left: 0.61 cm, No bullets or numbering

Deleted: summarizes

Deleted: (

Deleted: , ¶

Deleted: production

Deleted: such

434 Ireland. It is duly noted that NO<sub>x</sub> driven O<sub>3</sub> removal dominates over photochemical production  
 435 in these sites. A comparable study in the UK carried out by Finch and Palmer (2020) attributed  
 436 similarly rising trends in surface O<sub>3</sub> between 1999 and 2019 to decreasing NO<sub>x</sub>, characterising  
 437 UK observation sites as VOC-limited. Mixed results are observed at the urban stations of Cork,  
 438 with a positive trend at the South-link Road and Bishopstown, but a negative trend at the UCC  
 439 station. The UCC station, although classified as urban, lies within the university campus;  
 440 hence, it would not be subject to significant local emissions. Coastal sites like Mace Head and  
 441 Valentia generally show decreasing trends, potentially due to less local emission sources but  
 442 with more significant impacts from regional and long-range transport, However, a detailed  
 443 analysis of the trends requires consideration of seasonal effects.

Deleted: .

Deleted: This suggests variable factors affecting Cork O<sub>3</sub> levels...

444 Previous studies indicate that in northeast Europe, peak surface ozone concentrations have  
 445 generally declined, reflecting the effectiveness of emission control measures (Yan et al., 2018).  
 446 In contrast, background and lower-level O<sub>3</sub> concentrations have continued to increase,  
 447 particularly at rural and suburban sites. Consistent with this, urban observations from 2000–  
 448 2021 show increasing trends in median and lower-percentile O<sub>3</sub> levels, while the highest  
 449 extremes have mostly decreased (Nelson et al., 2025).

Formatted: Indent: Left: 0.01 cm, Right: 0 cm, Space After: 8.1 pt, Line spacing: Double

Formatted: Font colour: Blue

450 **Table 2.** - Trends in surface O<sub>3</sub> concentration (µg/m<sup>3</sup> per year) calculated for 13 sites in Ireland  
 451 over different periods over the complete dataset: 5 years (2018-2022), 10 years (2013-2022),  
 452 15 years (2008-2022), and the available measurement record for the site. The p-value evaluates  
 453 the reliability of the trend, whereas a lower p-value indicates trend certainty. Adopting the trend  
 454 reliability scale defined for TOAR-II studies (Chang et al., 2023), trends with very high  
 455 certainty will be marked by \*\*\* (p ≤ 0.001), trends with high certainty with \*\* (p ≤ 0.01), and  
 456 low to medium certainty with \* (p ≤ 0.05).

Formatted: Indent: Left: 0 cm, Right: 0 cm, Space After: 8.1 pt

Site No	Site name (Classification)	Measurement Record	Trend over record µg/m <sup>3</sup> per year	5-year trend 2018-2022 µg/m <sup>3</sup> per year	10-year trend 2013-2022 µg/m <sup>3</sup> per year	15-year trend 2008-2022 µg/m <sup>3</sup> per year
1	Mace Head (C)	1994-2022	0.02	-0.25	-0.31***	-0.11*

<u>2</u>	<u>Valentia (C)</u>	<u>2001-2022</u>	<u>-0.23****</u>	<u>-1.15****</u>	<u>-0.84****</u>	<u>-0.32***</u>
<u>3</u>	<u>Monaghan (R)</u>	<u>1995-2022</u>	<u>-0.19****</u>	<u>-0.74**</u>	<u>-0.35**</u>	<u>-0.09*</u>
<u>4</u>	<u>Laois (R)</u>	<u>2005-2022</u>	<u>0.39****</u>	<u>-0.15</u>	<u>0.3**</u>	<u>0.46****</u>
<u>5</u>	<u>Kilkenny (R)</u>	<u>2012-2022</u>	<u>0.02</u>	<u>-0.29</u>	<u>-0.01</u>	
<u>6</u>	<u>Castlebar (R)</u>	<u>2009-2022</u>	<u>0.18**</u>	<u>-0.71**</u>	<u>-0.05</u>	
<u>7</u>	<u>Rathmines (U)</u>	<u>2002-2022</u>	<u>0.27****</u>	<u>1.72****</u>	<u>1.15****</u>	<u>0.48****</u>
<u>8</u>	<u>Clonskeagh (U)</u>	<u>2008-2022</u>	<u>0.33****</u>	<u>0.97***</u>	<u>0.12</u>	<u>0.33****</u>
<u>9</u>	<u>Swords (U)</u>	<u>2009-2022</u>	<u>0.6****</u>	<u>0.07</u>	<u>0.33****</u>	
<u>10</u>	<u>Wicklow Bray (U)</u>	<u>2009-2022</u>	<u>0.14*</u>	<u>0.04</u>		
<u>11</u>	<u>Cork Southlink Road (U)</u>	<u>2014-2022</u>	<u>0.51*</u>	<u>-0.44</u>		
<u>12</u>	<u>Cork Bishopstown (U)</u>	<u>2016-2022</u>	<u>1.05****</u>	<u>-1.81*</u>		
<u>13</u>	<u>Cork UCC (U)</u>	<u>2018-2022</u>	<u>-0.94</u>	<u>-0.94</u>		

460

461

### 462 3.2.2 Monthly trend

463 Figure 3. shows the monthly trend for 10 years from the period 2012-2022. Mace Head  
464 (coastal) and Monaghan (rural) sites predominantly show a rising trend in winter/early spring,  
465 with a decreasing trend in late spring to summer. Valentia shows a decreasing trend in every  
466 month except February when levels are significantly impacted by long-range transport and  
467 stratospheric sources (Auvray and Bey, 2005; Pan et al., 2018). Urban sites show a general  
468 increasing monthly trend, as yearly trend but with a seasonal signal in Clonskeagh with an  
469 increase in winter-spring and a decrease in late spring or summer. Laois is characterised as a  
470 rural site yet exhibits rising trends similar to the urban sites for all months except December.

Deleted: Site c  
No

Formatted: Indent: Left: 0 cm, Right: 0 cm

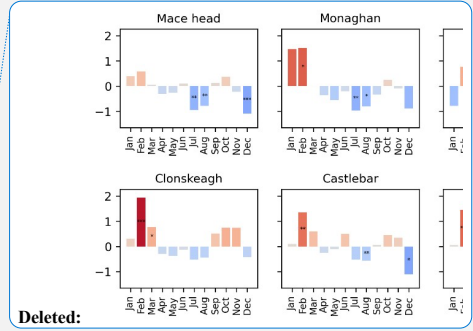
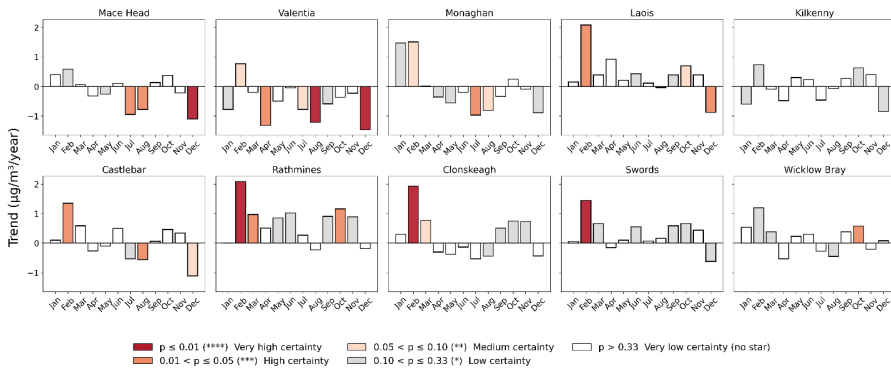
Deleted:

474 [indicating that the measurement station is affected by nearby emissions](#). Seasonal trends of the  
 475 15-year dataset are supplied in supplementary [Figure S2](#), where coastal stations exhibit a  
 476 pronounced increase in [late winter](#), and a decrease in late summer, with a consistent near-year-  
 477 round increase in [Rathmines and Laois](#).

Deleted: figure

Deleted: early spring

Deleted: urban stations of



Deleted:

478  
 479 **Figure 3.** Monthly trend analysis of O<sub>3</sub> at different sites for 10 year period. (2012-2022)  
 480 Adopting the trend reliability scale defined for TOAR-II studies (Chang et al., 2023), trends  
 481 significance highlighted by colour.

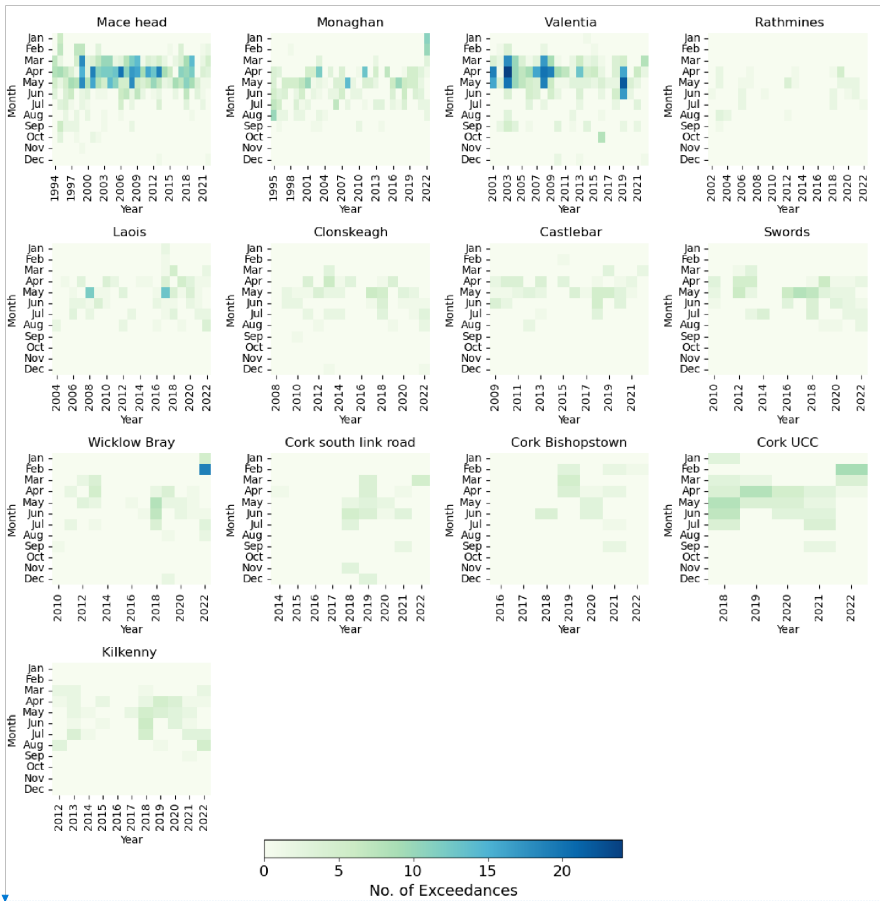
482 **3.3 O<sub>3</sub> Exceedance**

483 The O<sub>3</sub> exceedances at 13 sites in Ireland over the available measurement dataset [are identified](#)  
 484 [according to WHO criteria, and the results are shown in Figure 4](#). The highest and lowest  
 485 numbers of O<sub>3</sub> exceedances were observed at Mace Head and Rathmines, representing coastal  
 486 and urban sites, respectively. Most exceedances occurred in spring ([March, April May](#)),  
 487 [coinciding with the spring-time maximum](#). Rathmines had its highest number of exceedances  
 488 [in April 2019, while Laois reached a peak of 13 exceedances in May 2017](#). [Castlebar and](#)  
 489 [Swords show increased exceedance occurrences in spring and early summer, particularly](#)  
 490 [notable spikes occurring in 2010, 2013, 2016, and 2019](#). Conversely, Wicklow Bray exhibited

Deleted: **Figure 3.** Monthly trend analysis of O<sub>3</sub> at different sites for 10 year period. (2012-2022) Adopting the trend reliability scale defined for TOAR-II studies (Chang et al., 2023), trends with very high certainty are marked by \*\*\* (p ≤ 0.001), trends with high certainty with \*\* (p ≤ 0.01), and low to medium certainty with \* (p ≤ 0.05). Positive trends are in red shade and negative trends are in blue shade.

Deleted: O<sub>3</sub> exceedance are identified according WHO criteria and the results shown in figure 4. It shows the monthly

507 a different pattern, showing significant spikes in February and March 2022, alongside  
508 occasional exceedances during March, April, and May, for example, in 2012 and 2018. Cork  
509 South link Road also recorded exceedances, particularly in March and notably in June. Cork  
510 Bishoptown shows exceedances, especially in February and March 2019, while Cork UCC  
511 recorded exceedances in April and May 2019. Kilkenny consistently exhibited exceedances  
512 during spring and summer, with April and May often recording the highest numbers,  
513 particularly in 2019. This highlights the impact of seasonal atmospheric conditions on O<sub>3</sub>  
514 levels. It is noted that summertime exceedances, although less frequent in occurrence, indicate  
515 photochemical production events that would be required to elevate O<sub>3</sub> levels from the annual  
516 dip in the seasonal cycle to exceed the WHO AQG threshold. These episodic spikes are  
517 characteristic of unique climatic or pollution events and warrant further study.



518  
 519 **Figure 4.** - Monthly O<sub>3</sub> exceedance at different sites in Ireland. Exceedances are defined as  
 520 days on which the maximum 8-hour running average of ozone (O<sub>3</sub>) exceeds 100 µg/m<sup>3</sup>.

521 Figure 5 depicts trends in NO<sub>2</sub> and CH<sub>4</sub> concentrations across various Irish measurement sites.  
 522 NO<sub>2</sub> trend calculations are based on site-specific data periods , Cork South link Road (2014–  
 523 2022), Ballyfermot (2003–2022), Davit Road (2018–2023), Rathmines (1995–2024), Swords  
 524 (2011–2025), Laois (2014–2026), Castlebar (2003–2027), Louth Dundalk (2019–2028), and  
 525 Monaghan (2001–2029). For CH<sub>4</sub>, the data cover the period 2010–2022. Most monitored sites  
 526 exhibit a decreasing trend in NO<sub>2</sub> concentrations, most likely in response to pollution control

**Deleted:** when O<sub>3</sub> concentrations were at a maximum. ¶  
 Most sites recorded elevated spring-time occurrence in exceedances. E.g. Rathmines had its highest number of exceedances in April 2019, while Laois reached a peak of 13 exceedances in May 2017. Castlebar and Swords show increased exceedance occurrences in spring and early summer, particularly notable spikes occurring in 2010, 2013, 2016, and 2019. Conversely, ¶  
 Wicklow Bray exhibited a different pattern, showing significant spikes in February and March 2022, alongside occasional exceedances during March, April, and May, for example, in 2012 and 2018. Cork South link Road also recorded exceedances, particularly in March and June, with significant spikes in 2018 and 2019. Cork Bishopstown shows exceedances, especially in ¶  
 February and March 2019, while Cork UCC experienced spikes, particularly in April and May ¶  
 2019. Kilkenny consistently exhibited exceedances during spring and summer, with April and May often recording the highest number, particularly in 2019. This highlights the impact of seasonal atmospheric conditions on O<sub>3</sub> levels. It is noted that summertime exceedances, although less frequent in occurrence, indicate significant photochemical production that would be required to elevate O<sub>3</sub> levels from the annual dip in the seasonal cycle to exceed the WHO AQG threshold. These episodic spikes are characteristic of unique climatic or pollution events and warrant further study. ¶

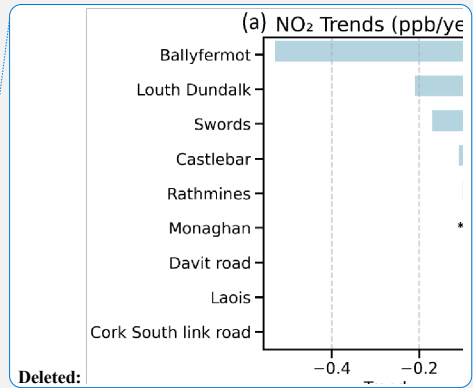
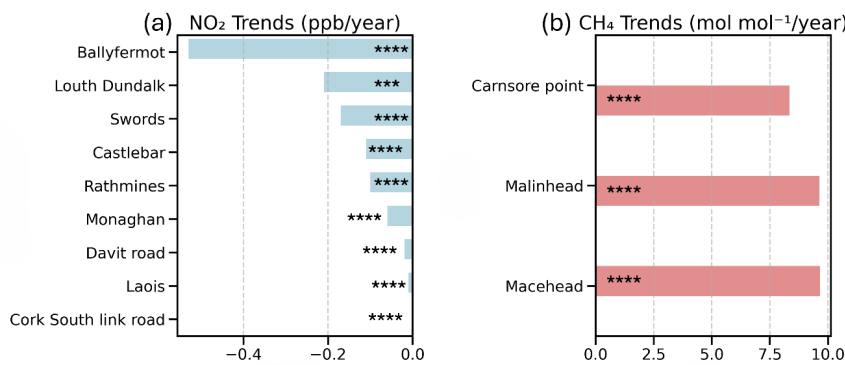
**Deleted:** ¶

**Formatted:** Indent: Left: 0 cm, First line: 0 cm, Right: 0 cm

**Deleted:** because of

556 on transportation, industrial activities, and energy production in the EU and North America,  
 557 (Coleman et al., 2013; Donlon et al., 2024). In contrast, CH<sub>4</sub> levels observed at three sites -  
 558 Mace Head, Malin Head, and Carnsore Point indicate a significant and persistent rise in CH<sub>4</sub>  
 559 concentrations. Mace Head is known for its clean Atlantic air and Malin Head, situated at  
 560 Ireland's northern tip near the UK border, offers a unique position to observe both clean marine  
 561 air and transboundary pollution whereas Carnsore Point in the southeast, is capture air masses  
 562 from both the UK and mainland Europe (Spohn et al., 2022). These NO<sub>2</sub> and CH<sub>4</sub> trends reveal  
 563 a dual dynamic: while NO<sub>2</sub> levels are decreasing due to effective emission controls, CH<sub>4</sub> levels  
 564 relentlessly rise, highlighting the need for enhanced mitigation strategies targeting CH<sub>4</sub>.

Deleted: ¶  
 Deleted: , in line with previous studies  
 Deleted:  
 Deleted: ,  
 Deleted: .  
 Deleted:  
 Deleted: , Carnsore Point receives the majority of air masses from the land  
 Deleted: are rising unabated



566  
 567 **Figure 5.** Trend in O<sub>3</sub> precursors NO<sub>2</sub> (a), and CH<sub>4</sub> (b) at different sites. Statistical significance  
 568 of trend is indicated, increasing \* with increasing trend reliability, as in Table 1.

Deleted: -  
 Formatted: Indent: Left: 0 cm, Right: 0 cm  
 Deleted: Trends with very high certainty are marked by \*\*\* (p ≤ 0.001), , trends with high certainty with \*\* (p ≤ 0.01),, and low to medium certainty with \* (p ≤ 0.05).

569 To evaluate the relationship between NO<sub>x</sub> and O<sub>3</sub> concentrations in an Irish context and the  
 570 potential benefit of abrupt enforcement of NO<sub>x</sub> control measures, we assess the impact of the  
 571 COVID-19 2020 lockdown, Spring 2020, whereby the lockdown period saw a prominent  
 572 relative decrease in NO<sub>2</sub>, yet an increase in surface O<sub>3</sub> compared to average measurements for  
 573 the same months 2017-2019 in most national monitoring stations (Figure 6). The negative

588 correlation between O<sub>3</sub> and NO<sub>2</sub> is indicative of a NO<sub>x</sub>-saturated regime, normally associated  
589 with polluted urban environments and NO<sub>x</sub> titration events. [Analysis of the impact of the](#)  
590 [lockdown on Irish O<sub>3</sub> is](#) discussed by Spohn et al. (2022), and a similar O<sub>3</sub> decrease was widely  
591 [observed across Europe](#) during the COVID lockdown (Ordóñez et al., 2020; Tavella & da Silva  
592 Júnior, 2021; C. Zhang & Stevenson, 2022). [Significant enhancement of O<sub>3</sub> occurs at the inland](#)  
593 [measurement sites, despite a 2020 springtime decrease in O<sub>3</sub> observed at background coastal](#)  
594 [sites, Mace Head and Valentia. These coastal stations are less sensitive to changes in European](#)  
595 [NO<sub>x</sub> emissions than inland sites and more sensitive to stratospheric and hemispheric transport](#)  
596 [\(Tan et al., 2018\). It is noted that April and May 2020 had unique meteorological conditions](#)  
597 [compared to previous years, with lower wind speed, less rain and significantly higher solar](#)  
598 [radiation, see Figure 12 in Spohn et al. \(2022\). These meteorological conditions would](#)  
599 [potentially facilitate photochemical O<sub>3</sub> production, contributing to positive O<sub>3</sub> anomalies](#)  
600 [during the lockdown period in addition to NO<sub>x</sub> reduction, also potentially enhancing dry](#)  
601 [deposition to the ocean. Further investigation into this topic would warrant model sensitivity](#)  
602 [studies, beyond the scope of this current work.](#)  
603 [The negative correlation between NO<sub>x</sub> and O<sub>3</sub> under relatively clean atmospheric conditions](#)  
604 [indicates that O<sub>3</sub> levels are influenced predominantly by transport and chemical removal, and](#)  
605 [local photochemical production does not represent a significant surface O<sub>3</sub> source owing to](#)  
606 [periods of low-insolation periods and low temperature, which are characteristic of Irish](#)  
607 [meteorology and frequent cloud cover \(Pallé and Butler, 2002\)](#)

**Deleted:** Similar results are

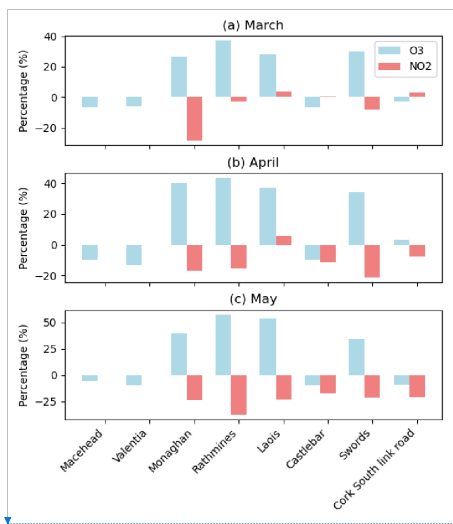
**Deleted:** (

**Deleted:** ,

**Formatted:** Subscript

**Formatted:** Subscript

**Deleted:** with meteorology. This effect was widely



**Deleted:** Significant enhancement of O<sub>3</sub> occurs at the inland measurement sites, despite a 2020 spring-time decrease in O<sub>3</sub> observed at background coastal sites, Mace Head and Valentia. These coastal stations are less sensitive to changes in European NO<sub>x</sub> emissions than inland sites and more sensitive to stratospheric and hemispheric transport (Tan et al., 2018) ¶

The atmospheric conditions in Ireland do not align with the interpretation of the atmosphere as being either a NO<sub>x</sub>-controlled regime for clean environments or a NO<sub>x</sub>-saturated regime in polluted environments. The negative correlation between NO<sub>x</sub> and O<sub>3</sub>, due to NO<sub>x</sub> titration, observed in Ireland occurs under relatively clean atmospheric conditions, but it is consistent with low-insolation conditions, which are characteristic of Irish meteorology and frequent cloud cover ((Pall E E and Butler, n.d.) ¶

612  
613

614 **Figure 6.** Percentage change in NO<sub>2</sub> and O<sub>3</sub> during the lockdown period of 2020 as compared  
615 to the 2017-2019 average at different sites in Ireland for (a) March (b) April (c) May.

**Deleted:** -  
**Formatted:** Indent: Left: 0 cm, Right: 0 cm  
**Deleted:**  
**Deleted:** April  
**Deleted:** Month  
**Deleted:** .

616 **3.4 Model and Observations Comparison**  
617 **3.4.1 Comparison between CAM4 – Chem Model and Observations**

618 Global simulations were performed with the CAM4-Chem model enabled with source tagging  
619 (Butler et al., 2018) for 2000-2018 and the modelled O<sub>3</sub> over Ireland was compared with  
620 surface O<sub>3</sub> measurements at five sites. [The grid details are shown in Figure S5. This model has](#)  
621 [already been comprehensively evaluated on a global scale \(Nalam et al., 2025\) against the](#)  
622 [TOAR-1 dataset, whereby the model performed well, albeit with a high bias attributable to the](#)  
623 [model's coarse resolution and implications for the resolution of urban chemistry \(Ansari et al.,](#)  
624 [2025\).](#) Figure 7 shows the comparison of monthly O<sub>3</sub> CAM4-Chem and ground station O<sub>3</sub> data.  
625 From this figure, it is observed that CAM4-Chem exhibits negative (positive) bias in rural and  
626 coastal (urban) sites. The underestimation at Mace Head is probably caused by the coarse grid  
627 resolution, covering a large area not representative of Mace Head conditions.

649 The influence of coastal meteorology, which suppresses O<sub>3</sub> formation due to cooler  
 650 temperatures and persistent cloud cover (McVeigh et al., 2010), also leads to an  
 651 underestimation of O<sub>3</sub> (Yerramilli et al., 2012). The dry deposition rate over land would exceed  
 652 that over the ocean, leading to a lower simulated O<sub>3</sub> concentration for the grid cell which covers  
 653 both land and ocean surface. Dry deposition is enhanced by solar radiation (Coleman et  
 654 al., 2012; Coleman et al., 2013; Pio et al., 2000) hence model measurement discrepancy is at a  
 655 maximum in late summer months. As outlined by Fiore et al. (2009), models average the  
 656 landscape characteristics within a grid cell, which can enhance O<sub>3</sub> deposition and result in  
 657 lower simulated O<sub>3</sub> concentrations; hence, the discrepancy is more pronounced in the clean  
 658 sector data.

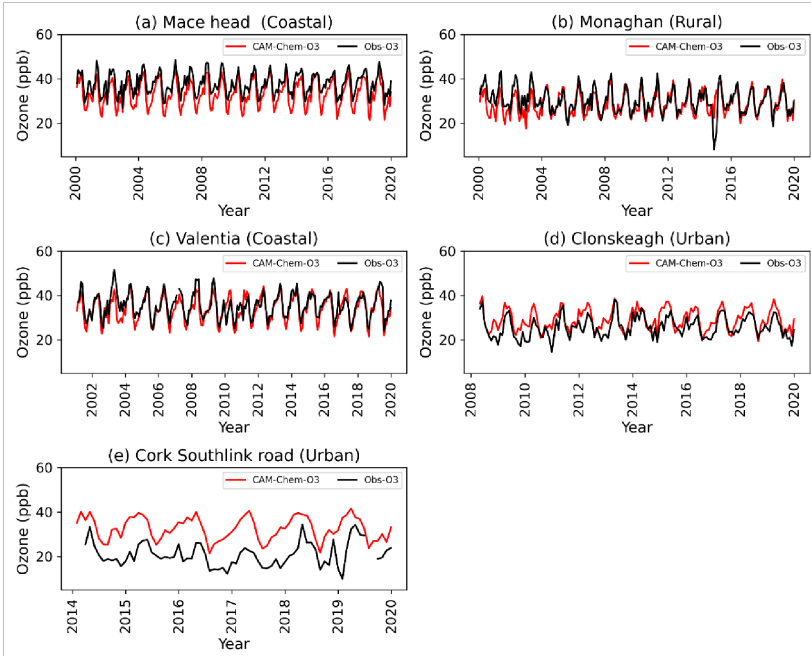
659 Overestimation of O<sub>3</sub> in Clonskeagh and Cork South link Road is likely due to coarse grid  
 660 handling of localised emissions and subsequent atmospheric chemistry.

**Deleted:** also leads to an underestimation of O<sub>3</sub> (Yerramilli et al 2012 ). Coastal meteorology, including cool sea surface temperatures and persistent clouds, suppresses O<sub>3</sub> formation. McVeigh et al., 2010 explained this through eddy correlation measurements showing downward ozone fluxes over coastal waters west of Ireland.

**Deleted:** The dry deposition rate over land would exceed that over the ocean leading to a lower simulated O<sub>3</sub> concentration for the entire grid cell.

**Formatted:** Indent: Left: 0 cm, Right: 0 cm

661



662

672 **Figure 7.** The comparison of Monthly CAM4 – Chem O<sub>3</sub> and Monthly O<sub>3</sub> observations at  
 673 five sites in Ireland.

674 At Mace Head, the model shows a negative mean bias of - 4.42 (-11.68% normalized mean  
 675 bias) but strong correlation (r =0.83). In Monaghan and Valentia, the model shows smaller  
 676 biases of -1.43 and -1.54, normalized mean biases of -4.74% and -1.54%, and correlation  
 677 coefficients of 0.73 and 0.72, respectively. These high correlations are in line with (Tilmes  
 678 et al., 2015). However, at Clonskeagh and Cork South Link Road, the model overestimates,  
 679 with positive biases (3.38 and 11.98) and weaker correlations (0.68 and 0.49). Statistics are  
 680 given, in more detail in the supplementary material [Table S1](#). These results suggest better  
 681 model performance at coastal/rural sites and greater discrepancies in areas affected by local  
 682 sources, as expected at this model resolution.

### 683 3.4.2 Source attribution using CAM4-Chem

684 To quantify the contribution of various precursor emission sources to modelled O<sub>3</sub>  
 685 concentrations, the TOAST1.0 dual NO<sub>x</sub> and VOC tagging technique was utilised (Butler et  
 686 al., 2018). This allows attribution of modelled O<sub>3</sub> to the emissions of NO<sub>x</sub> and VOC precursors  
 687 across different source sectors and geographical regions as listed in Table 3.

688 **Table 3.** - List of tags used in NO<sub>x</sub> and VOC tagging.

Regional Land-Based Tags		Regional Oceanic Tags		Global Sector/ProcessBased Tags	
<b>ARC</b>	Arctic	<b>NAL</b>	North Atlantic	<b>AIR</b>	Aircraft
<b>CAS</b>	Central Asia	<b>ENA</b>	Eastern North Atlantic	<b>BIO</b>	Biogenic
<b>EAS</b>	East Asia	<b>NAE</b>	North America East Coast	<b>BMB</b>	Biomass Burning
<b>EUR</b>	Europe	<b>NAW</b>	North American West Coast	<b>LGT</b>	Lightning

Deleted: -

Deleted: discussed

Deleted: table

Deleted: urban

Deleted: is utilised as described in ¶ (Butler et al., 2018). This allows us to attribute the modelled O<sub>3</sub> to the emissions of NO<sub>x</sub> and ¶ VOC precursors across different source sectors and regions as listed in Table 3. The NO<sub>x</sub> and VOC precursor emissions across different source sectors and regions, as shown in the Table, are responsible for the attribution of the modelled O<sub>3</sub>. ¶

<b>MCA</b>	Mexico & Central America	<b>NPA</b>	North Pacific	<b>STR</b>	Stratospheric Intrusion
<b>MDE</b>	Middle East	<b>BNS</b>	Baltic and North Seas	<b>XTR</b>	Extra untagged O <sub>3</sub>
<b>NAF</b>	North Africa	<b>HBV</b>	Hudson Bay	<b>CH4</b>	Methane
<b>NAM</b>	North America	<b>IDO</b>	Indian Ocean	<b>OCN</b>	Oceanic Sources (DMS)
<b>RBV</b>	Russia-BelarusUkraine	<b>MBC</b>	Mediterranean, Black, and Caspian Seas	<b>SHV</b>	Shipping
<b>SAS</b>	South Asia	<b>SHO</b>	Southern hemispheric oceans	<b>AIR</b>	Aircraft
<b>SEA</b>	Southeast Asia			<b>INI</b>	InitialConditionO <sub>3</sub>
<b>VRW</b>	Rest of the World				

700 The monthly tagged major precursor contributions to surface O<sub>3</sub> at Mace Head, averaged  
701 over the 2000-2018 simulation period, are shown in Figure 8. The stratospheric source of O<sub>3</sub>  
702 dominates in Winter-Spring, contributing to the spring-time maxima due to vigorous  
703 stratospheric transport. European NO<sub>x</sub> emissions contribution peaks in May, while lightning  
704 NO<sub>x</sub> has the greatest impact in winter. North American (NAM) NO<sub>x</sub> emissions contribute 3.5  
705 to 5.25 ppb, comparable to European NO<sub>x</sub>, but with an earlier peak in April. Aviation  
706 emissions contribute 1 to 3 ppb, with the highest contributions in winter and spring. Biogenic  
707 NO<sub>x</sub>, significant between June and October, contributes an average of 3.6 ppb, with higher  
708 contributions during August and September. O<sub>3</sub> derived from biogenic VOC sources average  
709 over 4 ppb during late autumn, maintaining a more sustained contribution throughout the  
710 year. East Asian NO<sub>x</sub> emissions, contribute up to 3.6 ppb, with a minimum contribution in  
711 July and August. North Atlantic shipping NO<sub>x</sub> (NAL) accounts for up to 2.4 ppb of O<sub>3</sub> during  
712 July. The total shipping NO<sub>x</sub> (SHIP) also contributes significantly. It is the addition of all  
713 oceanic emissions and shows the highest contribution in June.

Formatted: Subscript

Deleted: , peaking in April, and aviation

Deleted: Biogenic

Deleted: contribute slightly more, averaging

Deleted: and

Deleted: contributing

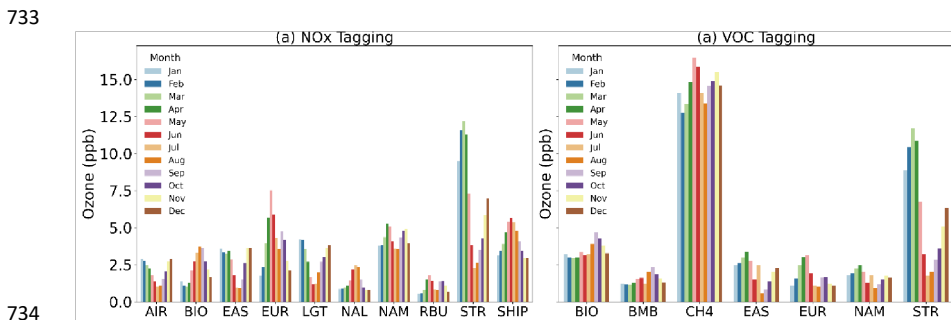
Deleted: show

Deleted: month

Deleted: and shows the highest contribution in June month.

723 Methane (CH<sub>4</sub>) is the dominant reactive carbon molecule contributing to O<sub>3</sub> formation. VOC  
 724 emissions from biomass burning also play a measurable role, contributing 1 to 2 ppb, with  
 725 their largest contributions in August and September. Finally, European VOC emissions  
 726 contribute 1 to 3 ppb, with the largest impact from March to May, coinciding with the spring-  
 727 time peak in surface O<sub>3</sub>.

728 These findings allow quantification of specific sources amidst the complex interplay of  
 729 regional and global sources in driving seasonal variations in surface O<sub>3</sub> levels over the Irish  
 730 domain, highlighting the roles of stratospheric processes, anthropogenic emissions, biogenic  
 731 sources, and lower-latitude contributions in shaping the observed patterns at background  
 732 monitoring sites such as Mace Head.



734  
 735 **Figure 8.-** Absolute contribution of major NO<sub>x</sub> sources (a) (NO<sub>x</sub> Tagging) and VOC source  
 736 (b) (NO<sub>x</sub> Tagging) to the CAM4-Chem simulated surface O<sub>3</sub> for the Mace Head grid cell  
 737 between 2000-2018.

738 Figure 9 shows the monthly changes in contributions to surface O<sub>3</sub> at Mace Head over the  
 739 simulation period (2000-2018). A negative (blue) trend indicates that the contribution of the  
 740 source to simulated surface O<sub>3</sub> in this grid cell has declined over the simulation period, whereas  
 741 a positive trend (red) indicates the contribution to surface O<sub>3</sub> has risen. Figure 9 (a) shows that  
 742 simulated O<sub>3</sub> at Mace Head originating from European or North American NO<sub>x</sub> decreases over

Formatted: Indent: Left: 0 cm, Right: 0 cm

Deleted: indicates

Deleted: the amount of

Deleted: during

746 the simulation period, consistent with EU & North American emission reductions, (Guerreiro  
747 et al., 2014). More significant reduction occurs in late Spring through late summer, when EU  
748 NO<sub>x</sub> contributions are most significant to Mace Head O<sub>3</sub> concentrations (as seen in Figure 8).

Deleted: over the period (,

Deleted: ;US EPA 2027

Deleted: , with m

Deleted: occurring

749 There is a rising trend in simulated surface O<sub>3</sub> originating from NO<sub>x</sub> emissions from global  
750 aviation, from East Asia, and to a lesser extent from South Asia, which is more pronounced in  
751 the wintertime. Wintertime temperatures in South Asia are still high enough to sufficiently  
752 produce local ozone, especially when NO<sub>x</sub> emissions are rising (Crippa et al., 2023). The  
753 relatively longer atmospheric lifetime of O<sub>3</sub> in the free troposphere during winter enables  
754 longer-range intercontinental transport (Huang et al., 2017; Yu et al., 2013). This seasonality  
755 in source contributions explains the observed reduction in spring-time maxima and increase in  
756 winter-time levels from the measurement record. EastAsian and South-Asian VOCs also  
757 contribute to a rising trend in simulated O<sub>3</sub>, with a more pronounced increase in winter and  
758 spring. This highlights a different pattern in hemispheric O<sub>3</sub> contributions, where EU and NAM  
759 emission reductions coincide with increased contribution from lower latitudes which could  
760 potentially become a more significant source of background O<sub>3</sub> in the Northern Hemisphere in  
761 the future. The contribution of CH<sub>4</sub> also has a positive trend over the simulation period, but the  
762 CH<sub>4</sub> trend has a reliable correlation only in the December and spring periods, with very low  
763 certainty in CH<sub>4</sub> contribution trends for summer months (correlation coefficient, p>0.33).  
764 Contribution to simulated O<sub>3</sub> at Mace Head from EU and NAM anthropogenic VOC show a  
765 negative trend for all months, consistent with trends from EU and NAM anthropogenic NO<sub>x</sub>.

Formatted: Indent: Left: 0 cm, Right: 0 cm, Space After: 8.1 pt, Line spacing: Double

Deleted: emission

Deleted: in Europe and North America are accompanied by

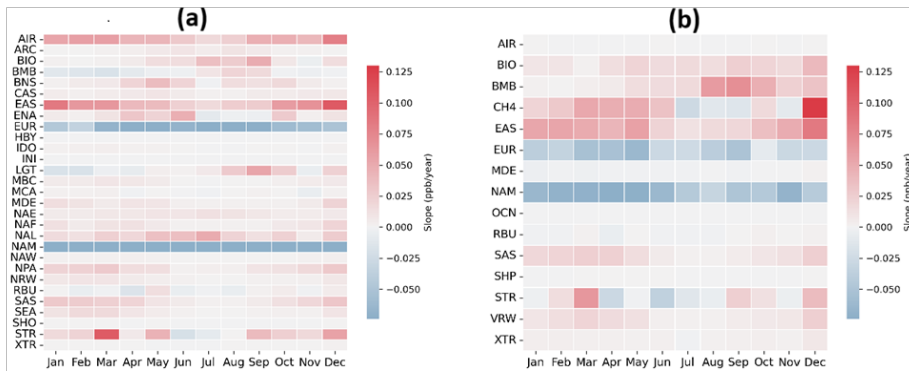
Deleted: influence

Deleted: . This increasing contribution could become a more important source of background O<sub>3</sub> in the future.

Deleted:

Deleted: no observed trend during the summer months when atmospheric CH<sub>4</sub> trends have very low certainty (correlation coefficient, p>0.33) consistent with decline in local NO<sub>x</sub> emissions in Europe.

Deleted: The Anthropogenic VOC contributions from Europe (EUR) and North America (NAM) show a negative trend for all months.



783  
784 **Figure 9.** Trends in contributions to monthly average modelled Mace Head grid cell surface  
785 O<sub>3</sub> at for the 2000-2018 period derived from (a) NO<sub>x</sub> tagging and (b)VOC tagging.

786 Table 4. shows the overall trend in the main contributors to NO<sub>x</sub> and VOC tagging. It is  
787 observed that there is an increase in simulated surface O<sub>3</sub> originating from NO<sub>x</sub> contributions  
788 from aviation and East Asia, while there is a decrease in European (EUR) and North American  
789 (NAM) NO<sub>x</sub> contributions. In VOC tagging, Methane (CH<sub>4</sub>) and East Asian anthropogenic  
790 VOC (EAS) contribute to a rising trend over the simulation period, whereas anthropogenic  
791 VOC contributions from Europe (EUR) and North America (NAM) show a negative trend.

792 **Table 4 - Overall Trend in contributions to Mace Head grid cell O<sub>3</sub> simulated by CAM4-**  
793 **Chem for NO<sub>x</sub> tagging and VOC tagging over the simulation period in units of ppb per year.**  
794 **reliability scale defined for TOAR-II studies (Chang et al., 2023). Statistical significance of**  
795 **trend is indicated using star notation: \*\*\*\* denotes  $p \leq 0.01$  (very high certainty), \*\*\* denotes**  
796  **$0.01 < p \leq 0.05$  (high certainty), \*\* denotes  $0.05 < p \leq 0.10$  (medium certainty), \* denotes**  
797  **$0.10 < p \leq 0.33$  (low certainty), and no star denotes  $p > 0.33$  (very low certainty).**

<b><u>NO<sub>x</sub> Tagging</u></b>		<b><u>VOC Tagging</u></b>	
	<b><u>Slope (ppb/year)</u></b>		<b><u>Slope (ppb/year)</u></b>

Formatted: Indent: Left: 0 cm, Right: 0 cm, Space After: 0.15 pt

Deleted: ,

Deleted: ¶

Deleted: ¶

Deleted: Overall Trend in contributions to Mace Head grid cell O<sub>3</sub> simulated by CAM4-Chem for NO<sub>x</sub> tagging and VOC tagging over the simulation period in units of ppb per year. The trend with very high certainty is marked by \*\*\*\*( $p \leq 0.001$ ), , trends with high certainty with \*\*( $p \leq 0.01$ ), and low to medium certainty with \*( $p \leq 0.05$ ).

<a href="#">AIR</a>	<a href="#">0.0467****</a>	<a href="#">CH<sub>4</sub></a>	<a href="#">0.0590****</a>
<a href="#">EAS</a>	<a href="#">0.0491****</a>	<a href="#">EAS</a>	<a href="#">0.0333****</a>
<a href="#">EUR</a>	<a href="#">-0.0900****</a>	<a href="#">EUR</a>	<a href="#">-0.0553****</a>
<a href="#">NAM</a>	<a href="#">-0.1243****</a>	<a href="#">NAM</a>	<a href="#">-0.0670****</a>

807

Deleted: ... [3]

808 **3.5 O<sub>3</sub> Trends in Background and EU influenced sector Airmasses at Mace Head**

809 Although Mace Head is classified as a global background site, quantification of the baseline  
810 pollution levels requires [trajectory analysis, whereby both measured and modelled data is](#)  
811 [filtered to limit the data to that arriving from the clean sector, unaffected by land-based](#)  
812 [emission sources, as discussed in Section 2.2. Figure 10 displays trends in observed and](#)  
813 [simulated O<sub>3</sub> at Mace Head, separated into seasons and clean/EU influenced sectors according](#)  
814 [to the trajectory analysis. The figure shows that the clean sector has consistently higher O<sub>3</sub>](#)  
815 [concentrations than the EU influenced sector for Winter, Spring and Autumn, with the most](#)  
816 [significant disparity between clean and EU sectors in winter/spring when stratospheric](#)  
817 [intrusion and lightning NO<sub>x</sub> contribute most significantly to O<sub>3</sub>, as discussed in Section 3.4.2.](#)  
818 [O<sub>3</sub> originating from EU airmasses is susceptible to higher rates of dry deposition and removal](#)  
819 [via local pollution while traversing the land-mass westwards towards Mace Head, leading to](#)  
820 [higher O<sub>3</sub> in clean-sector air masses consistent with previous studies \(Coleman et al., 2013\). A](#)  
821 [decreasing trend in mean spring-time levels is observed for both clean and EU influenced](#)  
822 [sectors, consistent with the sustained decrease in precursor emissions in Europe and North](#)  
823 [America as displayed in Figure 9. An increasing trend \(0.26 ppb/year\) is observed in the winter-](#)  
824 [time EU influenced sector, with a trend of smaller magnitude \(0.08 ppb/year\) observed in the](#)  
825 [clean sector, indicating a decrease in winter-time O<sub>3</sub> depletion events due to decreasing](#)

Deleted: filtering the data to limit the data to that arriving from the clean sector.

Deleted: ¶

830 [European emissions \(from the EU influenced sector\), consistent with the conclusions from](#)  
831 [previous studies of Mace Head surface O<sub>3</sub> \(Derwent et al., 2024\). Summer-time values do not](#)  
832 [exhibit a notable trend or a discrepancy between the clean and EU influenced sector](#)  
833 [measurements, indicating that there is little O<sub>3</sub> advected into Europe from the west in the](#)  
834 [summer months. It is noted that the seasonal trends exhibit slopes with p-values ranging](#)  
835 [between 0.1 > p > 0.01, which denote trends of medium to high certainty, as defined by TOAR](#)  
836 [assessment criteria of Chang et al., 2023.](#)

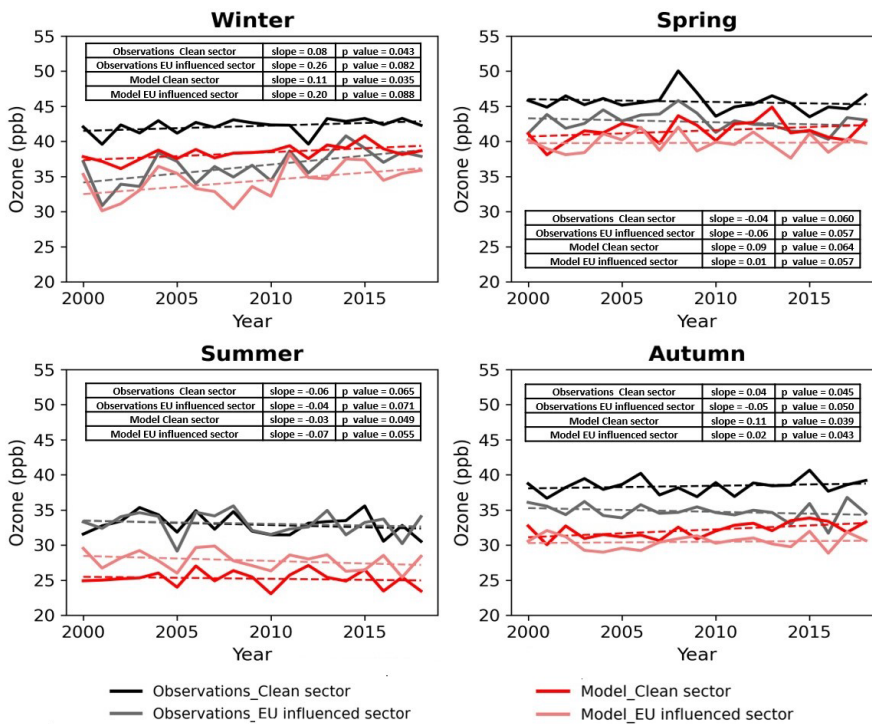
837 [Although the model results display a negative bias for reasons outlined in section 3.4.1, the](#)  
838 [clean sector consistently exhibits higher simulated O<sub>3</sub> concentrations than the EU-influenced](#)  
839 [sector, except during the summer season. In the winter season, a significant increasing trend is](#)  
840 [observed for simulated O<sub>3</sub> from both sectors, aligning with observations. A decreasing trend is](#)  
841 [observed during the summer season, again consistent with the observations for both sectors. In](#)  
842 [spring and autumn, modelled O<sub>3</sub> exhibits a positive trend over the simulation period.](#)

843 [Trends in contributors of model O<sub>3</sub> during the different seasons for the clean and EU-influenced](#)  
844 [sector are shown in Tables S3 to S4 in the supplementary material. Aviation and East Asian](#)  
845 [NO<sub>x</sub> show consistently positive and significant trends in both sectors, while North America](#)  
846 [NO<sub>x</sub> shows strong negative trends throughout the year in the clean sector. For the EU-](#)  
847 [influenced sector in NO<sub>x</sub> tagged \(Table S2\), similar positive trends observed for aviation and](#)  
848 [East Asian, with North America NO<sub>x</sub> remaining negative and European NO<sub>x</sub> showing more](#)  
849 [significant declines in spring and winter. In case of VOC tagged O<sub>3</sub>, the East Asian VOCs](#)  
850 [shows an increasing trend and North America VOCs show a negative across all seasons in both](#)  
851 [sectors \(Table S3 and S4\). European VOCs also show a consistent negative trend, particularly](#)  
852 [strong in the EU-influenced sector. Methane trends are seasonally positive, especially in spring](#)  
853 [and winter.](#)

854 It is observed that the model consistently simulates O<sub>3</sub> at lower concentrations than that  
 855 observed at Mace Head. This is not surprising, considering the coarse resolution of the model,  
 856 which limits its ability to represent fine-scale processes and dry deposition accurately. Dry  
 857 deposition is typically higher over land, and the grid cell covering Mace Head includes land  
 858 area, as shown in Figure S5 of the supplementary material. Further, as explained by Fiore et  
 859 al. (2009), models average the landscape characteristics within a grid cell, which can enhance  
 860 O<sub>3</sub> deposition and result in lower simulated O<sub>3</sub> concentrations; hence, the discrepancy is  
 861 more pronounced in the clean sector data.

**Deleted:** Based on the trajectories filtering of Mace head O<sub>3</sub> measurement data discussed in section 2.5. From figure 10 O<sub>3</sub> observations shows clean sector consistently has higher O<sub>3</sub> concentrations than the EU influenced sector especially during the annual spring-time high, indicating a longer lifetime for O<sub>3</sub> over the North Atlantic, and the land mass and pollution sources are acting as a sink for O<sub>3</sub> in the Irish context (Fowler et., al 2008). A decreasing trend in spring-time levels is observed for both clean and EU influenced sectors, consistent with the decrease in precursor emissions in Europe and North America. There is a significant difference between clean, and EU influenced sector measurements, the influence of EU influenced sector air to scavenge O<sub>3</sub> via NO<sub>x</sub> titration, leading to higher O<sub>3</sub> in clean-sector air masses, as also found in previous studies (Coleman et al., 2013). An increasing trend is observed in the winter-time EU influenced sector, which is not observed in the clean sector. This would infer a decrease in winter-time O<sub>3</sub> depletion events due to decreasing European emissions (from the EU influenced sector), consistent with the conclusions from previous studies of Mace Head surface O<sub>3</sub> (Derwent et al., 2024). Summer-time values do not exhibit a notable trend or a discrepancy between clean and EU influenced sector measurements, indicating that there is little O<sub>3</sub> advected into Europe from the west in the summer months. Autumn values show higher O<sub>3</sub> in the clean sector, but without a significant slope.

The model results indicate that the clean sector consistently exhibits higher O<sub>3</sub> concentrations than the EU-influenced sector, except during the summer season. In the winter season, a significant increasing trend is observed for both sectors, which aligns well with the O<sub>3</sub> observations. A decreasing trend is observed during the summer season, consistent with the observations for both sectors. In spring and autumn, a positive trend is observed. Trends in contributors of model O<sub>3</sub> during the different seasons for the clean and EU-influenced sector are shown in Tables S3 to S4 in the supplementary material. Aviation and East Asian NO<sub>x</sub> shows consistently positive and significant trends in both sectors, while North America NO<sub>x</sub> shows strong negative trends throughout the year in the clean sector. For the EU-influenced sector in NO<sub>x</sub> tagged (Table S2), similar positive trends observed for aviation and East Asian, with North America NO<sub>x</sub> remaining negative and European NO<sub>x</sub> showing more significant declines in spring and winter. In case of VOC tagged O<sub>3</sub>, the East Asian VOCs shows an increasing trend and North America VOCs negative across all seasons in both sectors (Table S3 and S4). European VOCs also show a consistent negative trend, particularly strong in the EU-influenced sector. Methane trends are seasonally positive, especially in spring and winter.



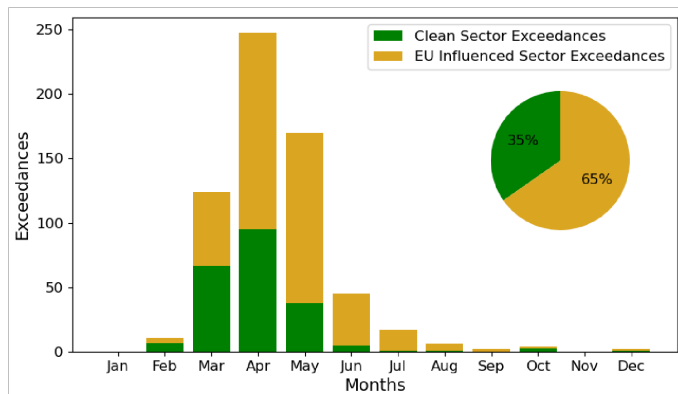
862  
 863 **Figure 10.** - Trend in seasonal Average of observed O<sub>3</sub> (black ) and Model O<sub>3</sub> (red) at Mace  
 864 head, separated into clean sector and EU-influenced sector.

916 **3.6 Exceedances from the clean and EU-influenced sector at Mace Head**

917 Exceedances observed at Mace Head between 2000 and 2022 are separated into clean and EU-  
918 influenced sectors based on trajectory air masses and shown in Figure 11. 35% of all  
919 exceedances for this period occurred in clean air masses, the remainder occurring when air  
920 masses include EU outflow and contribution from local sources to enhance surface O<sub>3</sub> at Mace  
921 Head, which is already elevated compared to inland and urban sites. It is notable that there is  
922 a higher proportion of exceedances that occur from EU- influenced sector, despite higher mean  
923 observations from the clean sector for all seasons. This occurs because of an enhancement of  
924 surface O<sub>3</sub> occur during an influx of polluted air from the EU, UK or local sources. The EU  
925 influence on exceedance becomes more proportionally prominent in late Spring and summer,  
926 with more frequent easterly airflow when there is a higher occurrence of stagnation events.

Deleted: 33

927 Deleted: O<sub>3</sub>-EU influenced sector air is advected over Ireland and local land masses to enhance surface O<sub>3</sub>, which is already elevated at Mace Head compared to inland and urban sites.

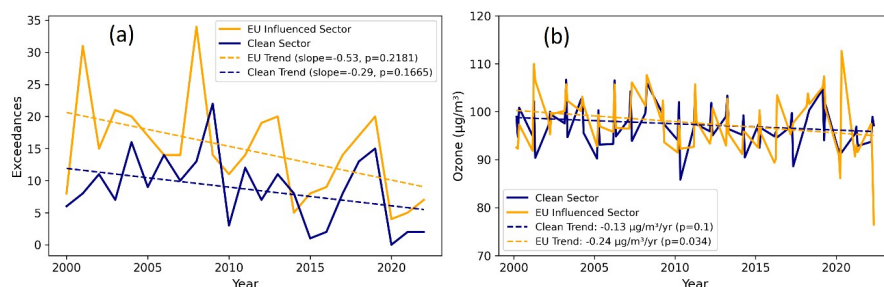


928  
929 **Figure 11.** - Exceedances measured at Mace Head per month from 2000 until 2022, during  
930 the clean air sector (green) and EU influenced sector (yellow). The percentage of both to total  
931 exceedances is shown in the inlay.

937 Figure 12 shows the trend in spring-time exceedances and the 95<sup>th</sup> percentile Spring-time O<sub>3</sub>  
 938 measured at Mace Head between 2000 and 2022. [A decreasing trend in exceedances is](#)  
 939 [observed, with a greater decreasing trend in from the EU and locally influenced sector.](#) This  
 940 indicates that the changes that are driving the reduction in the exceedances in Europe are  
 941 coming into effect at a quicker rate than the changes that are driving [the](#) O<sub>3</sub> event reduction  
 942 over the North Atlantic. The trends in the exceedance counts are not significant, according  
 943 to the criteria in Chang et al., 2023, but there is a statistically significant decreasing trend in  
 944 the 95<sup>th</sup> percentile springtime surface O<sub>3</sub> over the measurement record. Figure 12 (b) shows  
 945 the trend in spring-time surface O<sub>3</sub> measured at Mace Head segregated into Clean and EU-  
 946 influenced sector. The trend is more significant both in magnitude and statistical certainty  
 947 for the EU-influenced sector, indicating [that European](#) emission changes [have](#) a more  
 948 pronounced effect on springtime O<sub>3</sub> measured at Mace Head O<sub>3</sub> as compared to changes  
 949 affecting O<sub>3</sub> transported or formed over the North Atlantic.

**Deleted:** A decreasing trend in exceedances and clean sector spring-time exceedances is observed, with a greater decreasing trend in the total number of exceedances.

**Deleted:** EU  
**Deleted:** having  
**Deleted:** -



950 **Figure 12.** (a) The trend in Spring-time exceedances measured at Mace Head between 2000  
 951 and 2022 (blue) with the clean-air exceedances (gold), and (b) The trend in 95<sup>th</sup> percentile  
 952 of spring (Mar- May) O<sub>3</sub> measured in µg /m<sup>3</sup> for the clean sector (blue) and the EU-influenced  
 953 sector (gold).  
 954

955 [Figure 13 shows monthly cumulative contributions to simulated O<sub>3</sub> concentrations within the](#)  
 956 [Mace Head grid cell for NO<sub>x</sub> and VOC tagging during O<sub>3</sub> exceedance. First, the exceedances](#)

963 were identified from O<sub>3</sub> observations as discussed in Section 3.3 and then these exceedances  
964 were divided into two sectors the EU-influenced sector and the clean sector. In Figure 13, the  
965 hourly O<sub>3</sub> exceedance cumulative concentrations in ppb, along with the contributions from  
966 different parameters, are shown. It indicates which parameters contribute more to the  
967 exceedances, in both the EU-influenced sector or the clean sector. In this the ug/m3 to ppb  
968 conversion is considered for the exceedances.

969 These exceedances are categorised into clean and EU-influenced sectors. The maximum  
970 exceedances are observed in March to May. From Figure 13 (a), it is clear that stratospheric  
971 intrusion, North American NO<sub>x</sub>, European NO<sub>x</sub>, and East Asian NO<sub>x</sub> are the major  
972 contributors driving exceedances at Mace Head during the spring months (March to May).

973 European emissions dominate the supply of NO<sub>x</sub> precursors in April, reaching their peak in  
974 May. Figure 13 (b) shows that CH<sub>4</sub> is the most dominant VOC source, followed by stratospheric  
975 intrusion and Biomass burning. North American and European VOC emissions also contribute  
976 significantly to O<sub>3</sub> formation during this period. Collectively, these findings highlight the  
977 complex interplay of regional and global sources in driving surface O<sub>3</sub> exceedances over the  
978 Irish domain.

979 North American NO<sub>x</sub> also contributes significantly to exceedance in both clean and EU-  
980 influenced sectors at Mace Head during March to May month, likely due to long-range  
981 transport and mixing, regional stagnation or synoptic-scale recirculation. In the case of VOC  
982 tagging, stratospheric intrusion, and CH<sub>4</sub> show notable contributions. Biomass burning, East  
983 Asian emissions and North American VOC emissions also play a role in O<sub>3</sub> exceedances.

984 The IN\_SHIP indicates the total contribution of all international shipping emissions  
985 (ENA,NAE,NAW,NPA,BNS,HB,Y,IDO,MBC,SHO) which is significant in April and May.

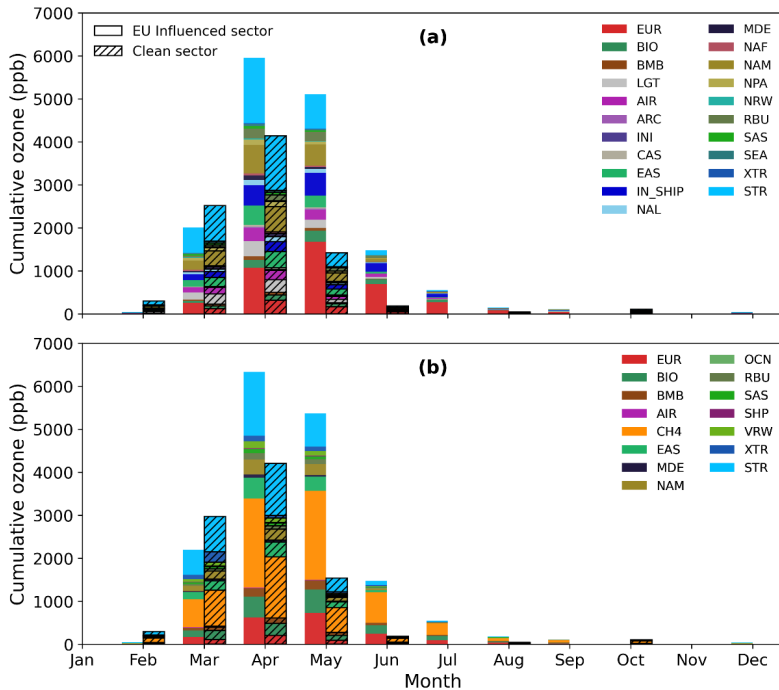
**Deleted:** Figure 13 shows monthly cumulative contributions to simulated O<sub>3</sub> concentrations within the Mace Head grid cell for NO<sub>x</sub> and VOC tagging during O<sub>3</sub> exceedance, which is observed from O<sub>3</sub> observations calculated as discussed in section 3.3. In addition, t

**Deleted:** ¶

**Deleted:** month

**Formatted:** Space After: 0 pt

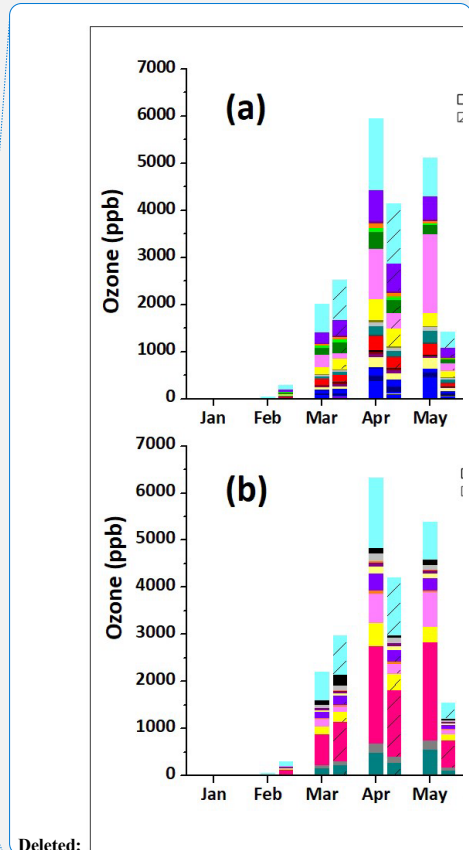
**Deleted:** Among these, European emissions dominate the supply of NO<sub>x</sub> precursors in April, reaching their peak in May. Figure ¶  
13 (b) shows that CH<sub>4</sub> is the most dominant source, followed by stratospheric intrusion and Biomass burning. North American and European VOC emissions also contribute significantly to O<sub>3</sub> formation during this period. Collectively, these findings highlight the complex interplay of regional and global sources in driving surface O<sub>3</sub> exceedances over the Irish domain. ¶  
The cumulative O<sub>3</sub> contributions to EU-influenced sector and clean sector exceedances for NO<sub>x</sub> tagging and VOC tagging, it is clear that the North American NO<sub>x</sub> also contributes significantly to exceedance in both clean and EU-influenced sectors at Mace Head during March to May months. It may be due to transport and mixing, regional stagnation or synopticscale recirculation



1010  
 1011 **Figure 13** - Monthly cumulative Mace Head grid cell O<sub>3</sub> contributions to EU influenced sector  
 1012 and clean sector exceedances (a) NO<sub>x</sub> tagging and (b) VOC tagging Mace Head grid cell.

1013 **4. Conclusion**

1014 This study highlights the complexities of O<sub>3</sub> pollution in Ireland, revealing that coastal areas  
 1015 experience higher O<sub>3</sub> concentrations than rural and urban environments, attributed to the effect  
 1016 of transboundary pollution and stratospheric intrusion. [Over the last two decades, urban sites](#)  
 1017 [have shown a significant increasing trend in O<sub>3</sub> levels, particularly in winter, influenced by](#)  
 1018 [decreasing anthropogenic pollution in Europe, the UK, North America and local to the](#)  
 1019 [observation sites, representing a decline in chemical removal mechanism \(Derwent et al., 2024;](#)  
 1020 [Simmonds and Derwent, 1991\). The analysis also points out that the majority of exceedances](#)  
 1021 [at coastal monitoring sites coincide with the annual spring maxima. Using the advanced](#)  
 1022 capabilities of the CAM4-Chem model with dual NO<sub>x</sub> and VOC tagging, we identified key



Deleted:

Deleted:

Formatted: Indent: Left: 0 cm, Right: 0 cm, Space After: 0.05 pt, Line spacing: Multiple 1.99 li

Deleted:

Deleted: ¶

Deleted: <#>

Deleted: <#>¶

Formatted: Indent: Left: 0 cm, Right: 0 cm

Deleted: Over the last two decades, urban sites have shown a significant increasing trend in O<sub>3</sub> levels, likely influenced by decreasing nitrogen oxides (NO<sub>x</sub>) in Europe, including Ireland, and North America. The analysis also points out that exceedances at coastal monitoring sites correlate with years of higher spring maxima, driven mainly by hemispheric transport and stratospheric influences(16%). Utilising

1036 factors affecting seasonal O<sub>3</sub> variations, such as the spring-time peak and summer dip, driven  
1037 by a mix of stratospheric intrusion, [NO<sub>x</sub> emissions from lightning, long range and hemispheric](#)  
1038 [transport, regional emissions and aviation related emissions](#). Trend analysis from simulation  
1039 results identified East Asian and aviation emissions as significant contributors to the rising  
1040 winter trends in O<sub>3</sub>, while reductions in North American and European emissions accounted  
1041 for the decrease in spring peaks. This study provides a comprehensive understanding of the  
1042 various factors affecting O<sub>3</sub> levels in Ireland, offering important insights for the development  
1043 of O<sub>3</sub> pollution control policies.

Deleted: hemispheric transport, and regional emissions

1044

#### 1045 **Data availability**

1046 All data are available upon request.

#### 1047 **Author contributions**

1048 LC designed the study. NK analyzed the data and wrote the manuscript. TA and TB  
1049 provided CAM-Chem model results and reviewed the manuscript.. JO and CD reviewed the  
1050 manuscript and edited it.LC edited it with contributions from all coauthors

#### 1051 **Competing interests**

1052 The authors declare that at least one of the authors sits on the editorial board of ACP.

1053 **Acknowledgement** - The authors acknowledge the Environmental Protection Agency (EPA)  
1054 of Ireland for their financial support of the Ozone project under the EPA Research  
1055 Programme  
1056 2021-2030 (project number 2022-CE-1133), and the European Union's Horizon Europe  
1057 Research and Innovation programme under HORIZON-CL5-2022-D1-02 (grant no.  
1058 101081430-PARIS).

1060

1061 **References**

1062 Aghedo, A. M., Bowman, K. W., Worden, H. M., Kulawik, S. S., Shindell, D. T., Lamarque,  
1063 J. F., Faluvegi, G., Parrington, M., Jones, D. B. A., and Rast, S.: The vertical distribution of  
1064 ozone instantaneous radiative forcing from satellite and chemistry climate models, *Journal*  
1065 *of Geophysical Research Atmospheres*, 116, <https://doi.org/10.1029/2010JD014243>, 2011.

1066 Anenberg, S. C., West, J. J., Fiore, A. M., Jaffe, D. A., Prather, M. J., Bergmann, D., Cuvelier,  
1067 K., Dentener, F. J., Duncan, B. N., Gauss, M., Hess, P., Jonson, J. E., Lupu, A., Mackenzie,  
1068 I.

1069 A., Marmer, E., Park, R. J., Sanderson, M. G., Schultz, M., Shindell, D. T., Szopa, S.,  
1070 Vivanco,

1071 M. G., Wild, O., and Zeng, G.: Intercontinental impacts of ozone pollution on human  
1072 mortality,

1073 *Environ Sci Technol*, 43, 6482–6487, <https://doi.org/10.1021/es900518z>, 2009.

1074 [Ansari, T., Nalam, A., Lupaşcu, A., Hinz, C., Grasse, S., & Butler, T.: Explaining trends and](#)  
1075 [changing seasonal cycles of surface ozone in North America and Europe over the 2000–2018](#)  
1076 [period: a global modelling study with NO<sub>x</sub> and VOC tagging. \*Atmospheric Chemistry and\*](#)  
1077 [Physics, 25, 16833–16833. <https://doi.org/10.5194/acp-25-16833-2025>.](#)

1078 [Archibald, A. T., Neu, J. L., Elshorbany, Y. F., Cooper, O. R., Young, P. J., Frost, G. J.,](#)  
1079 [Galbally, I. E., Gerosa, G., Granier, C., and Griffiths, P. T.: Tropospheric Ozone Assessment](#)  
1080 [Report : A critical review of changes in the tropospheric ozone burden and budget from 1850](#)  
1081 [to 2100, 1– 53, 2020.](#)

1082 Ashmore, M. R.: Assessing the future global impacts of ozone on vegetation, *Plant Cell*  
1083 *Environ*, 28, 949–964, <https://doi.org/10.1111/j.1365-3040.2005.01341.x>, 2005.

**Deleted:** Ansari, T., Nalam, A., Lupaşcu, A., Hinz, C., Grasse, S., and Butler, T.: Explaining trends and changing seasonal cycles of surface ozone in North America and Europe over the 2000–2018 [↗](#)  
period: → A → global → modelling → study → with → NO<sub>x</sub> →  
→ and → VOC → tagging, [↗](#)  
<https://doi.org/10.5194/egusphere-2024-3752>, 13 December 2024. [↗](#)

1092 Atkinson-Palombo, C. M., Miller, J. A., and Balling, R. C.: Quantifying the ozone “weekend  
1093 effect” at various locations in Phoenix, Arizona, *Atmos Environ*, 40, 7644–7658,  
1094 <https://doi.org/10.1016/j.atmosenv.2006.05.023>, 2006.

1095 Auvray, M. and Bey, I.: Long-range transport to Europe: Seasonal variations and implications  
1096 for the European ozone budget, <https://doi.org/10.1029/2004JD005503>, 16 June 2005.

1097 Bessagnet, B., Pirovano, G., Mircea, M., Cuvelier, C., Aulinger, A., Calori, G., Ciarelli, G.,  
1098 Manders, A., Stern, R., Tsyro, S., García Vivanco, M., Thunis, P., Pay, M. T., Colette, A.,  
1099 Couvidat, F., Meleux, F., Rouíl, L., Ung, A., Aksoyoglu, S., Baldasano, J. M., Bieser, J.,  
1100 Briganti, G., Cappelletti, A., D’Isidoro, M., Finardi, S., Kranenburg, R., Silibello, C.,

1101 Carnevale, C., Aas, W., Dupont, J. C., Fagerli, H., Gonzalez, L., Menut, L., Prévôt, A. S. H.,  
1102 Roberts, P., and White, L.: Presentation of the EURODELTA III intercomparison  
1103 exercise evaluation of the chemistry transport models’ performance on criteria pollutants and  
1104 joint analysis with meteorology, *Atmos Chem Phys*, 16, 12667–12701,  
1105 <https://doi.org/10.5194/acp-16-12667-2016>, 2016.

1106 [Bonaccorso, B., Peres, D. J., Cancelliere, A., and Di Mauro, G.: Probabilistic forecasting of  
1107 drought class transitions in Sicily \(Italy\) using Standardized Precipitation Index and North  
1108 Atlantic Oscillation Index, \*Hydrol. Earth Syst. Sci.\*, 19, 389–404, 2015.](#)

1109 Boylan, P., Helmig, D., and Oltmans, S.: Ozone in the Atlantic Ocean marine boundary layer,  
1110 1–13, <https://doi.org/10.12952/journal.elementa.000045>, 2014.

1111 Butchart, N., Charlton-Perez, A. J., Cionni, I., Hardiman, S. C., Haynes, P. H., Krüger, K.,  
1112 Kushner, P. J., Newman, P. A., Osprey, S. M., Perlwitz, J., Sigmond, M., Wang, L., Akiyoshi,  
1113 H., Austin, J., Bekki, S., Baumgaertner, A., Braesicke, P., Brhl, C., Chipperfield, M.,  
1114 Dameris,

1115 M., Dhomse, S., Eyring, V., Garcia, R., Garny, H., Jöckel, P., Lamarque, J. F., Marchand, M.,  
1116 Michou, M., Morgenstern, O., Nakamura, T., Pawson, S., Plummer, D., Pyle, J., Rozanov, E.,

Formatted: Space After: 0 pt, Line spacing: Multiple 1.99 li

Deleted: ¶

1118 Scinocca, J., Shepherd, T. G., Shibata, K., Smale, D., Teyssèdre, H., Tian, W., Waugh, D.,  
1119 and  
1120 Yamashita, Y.: Multimodel climate and variability of the stratosphere, *Journal of Geophysical*  
1121 *Research Atmospheres*, 116, <https://doi.org/10.1029/2010JD014995>, 2011.

1122 Butler, T., Lupascu, A., Coates, J., and Zhu, S.: TOAST 1.0: Tropospheric ozone attribution  
1123 of  
1124 sources with tagging for CESM 1.2.2, *Geosci Model Dev*, 11, 2825–2840,  
1125 <https://doi.org/10.5194/gmd-11-2825-2018>, 2018.

1126 Butler, T., Lupascu, A., and Nalam, A.: Attribution of ground-level ozone to anthropogenic  
1127 and natural sources of nitrogen oxides and reactive carbon in a global chemical transport  
1128 model, *Atmos Chem Phys*, 20, 10707–10731, <https://doi.org/10.5194/acp-20-10707-2020>,  
1129 2020.

1130 Carslaw, D. C.: On the changing seasonal cycles and trends of ozone at Mace Head, Ireland,  
1131 *Atmos. Chem. Phys*, 3441–3450 pp., 2005.

1132 Chang, K.-L., Schultz, M. G., Koren, G., and Selke, N.: Guidance note on best statistical  
1133 practices for TOAR analyses, 2023.

1134 [Coates, J., Mar, K. A., Ojha, N., & Butler, T. M.: The influence of temperature on ozone](#)  
1135 [production under varying NO x conditions—a modelling study. \*Atmospheric Chemistry and\*](#)  
1136 [Physics, 16\(18\), 11601-11615, 2016.](#)

1137 [Coleman, L., McVeigh, P., Berresheim, H., Martino, M., and O’Dowd, C. D.: Photochemical](#)  
1138 [impact on ozone fluxes in coastal waters, \*Advances in Meteorology\*, 2012,](#)  
1139 <https://doi.org/10.1155/2012/943785>, 2012.

1140 Coleman, L., Martin, D., Varghese, S., Jennings, S. G., and O’Dowd, C. D.: Assessment of  
1141 changing meteorology and emissions on air quality using a regional climate model: Impact

Deleted: ¶

1143 on ozone, *Atmos Environ*, 69, 198–210, <https://doi.org/10.1016/j.atmosenv.2012.11.048>,  
1144 2013.

1145 Creilson, J. K., Fishman, J., & Wozniak, A. E. Intercontinental transport of tropospheric  
1146 ozone: A study of its seasonal variability across the North Atlantic utilizing tropospheric  
1147 ozone residuals and its relationship to the North Atlantic Oscillation. *Atmospheric Chemistry  
1148 and Physics*, 3(6), 2053–2066. <https://doi.org/10.5194/acp-3-2053-2003>, 2003.

1149 [Crippa, M., Guizzardi, D., Butler, T. M., Keating, T., Wu, R., Kaminski, J., Kiesewetter, G.,  
1150 Im, U., Bessagnet, B., Chabrilat, S., et al.: The HTAP\\_v3 emission mosaic: merging regional  
1151 and global monthly emissions \(2000–2018\) to support air quality modelling and policies, \*Earth  
1152 Syst. Sci. Data\*, 15, 2667–2696, 2023.](#)

1153 [Crippa, M., Guizzardi, D., Pagani, F., Schiavina, M., Melchiorri, M., Pisoni, E., Graziosi, F.,  
1154 Muntean, M., Maes, J., Dijkstra, L., Van Damme, M., Clarisse, L., and Coheur, P.: Insights  
1155 into the spatial distribution of global, national, and subnational greenhouse gas emissions in  
1156 the  
1157 Emissions Database for Global Atmospheric Research \(EDGAR v8.0\), \*Earth Syst Sci Data\*,  
1158 16, 2811–2830, <https://doi.org/10.5194/essd-16-2811-2024>, 2024.](#)

1159 Derwent, R. G.: [Observation and interpretation of the seasonal cycles in the surface  
1160 concentrations of ozone and carbon monoxide at Mace Head, Ireland from 1990 to 1994,](#)  
1161 [Atmos Environ, 32, 2310, \[https://doi.org/10.1016/S1352-2310\\(97\\)00338-5\]\(https://doi.org/10.1016/S1352-2310\(97\)00338-5\), 1998.](#)

1162 Derwent, R. G., Simmonds, P. G., and Collins, W. J.: Ozone and carbon monoxide  
1163 measurements at a remote maritime location, mace head, Ireland, from 1990 to 1992, *Atmos  
1164 Environ*, 28, 2623–2637, [https://doi.org/10.1016/1352-2310\(94\)90436-7](https://doi.org/10.1016/1352-2310(94)90436-7), 1994.

1165 Derwent, R. G., Jenkin, M. E., Saunders, S. M., and Pilling, M. J.: Photochemical ozone  
1166 creation potentials for organic compounds in northwest Europe calculated with a master

Deleted: ¶

Deleted: OBSERVATION AND INTERPRETATION OF  
THE SEASONAL CYCLES ¶  
IN THE SURFACE CONCENTRATIONS OF OZONE  
AND CARBON MONOXIDE AT MACE HEAD ,  
IRELAND FROM 1990 TO 1994, 2310, 1998

1173 chemical mechanism, Atmos Environ, 32, 2429–2441,  
1174 [https://doi.org/10.1016/S13522310\(98\)00053-3](https://doi.org/10.1016/S13522310(98)00053-3), 1998.

1175 Derwent, R. G., Collins, W. J., Johnson, C. E., and Stevenson, D. S.: Transient behaviour of  
1176 tropospheric ozone precursors in a global 3-d ctm and their indirect greenhouse effects, 2001.

1177 Derwent, R. G., Stevenson, D. S., Collins, W. J., and Johnson, C. E.: Intercontinental  
1178 transport and the origins of the ozone observed at surface sites in Europe, Atmos Environ,  
1179 38, 1891–1901, <https://doi.org/10.1016/j.atmosenv.2004.01.008>, 2004.

1180 Derwent, R. G., Stevenson, D. S., Doherty, R. M., Collins, W. J., and Sanderson, M. G.: How  
1181 is surface ozone in Europe linked to Asian and North American NO<sub>x</sub> emissions?, Atmos  
1182 Environ, 42, 7412–7422, <https://doi.org/10.1016/j.atmosenv.2008.06.037>, 2008.

1183 Derwent, R. G., Manning, A. J., Simmonds, P. G., Spain, T. G., and O’Doherty, S.: Analysis  
1184 and interpretation of 25 years of ozone observations at the Mace Head Atmospheric Research  
1185 Station on the Atlantic Ocean coast of Ireland from 1987 to 2012, Atmos Environ, 80, 361–  
1186 368, <https://doi.org/10.1016/j.atmosenv.2013.08.003>, 2013.

1187 Derwent, R. G., Manning, A. J., Simmonds, P. G., and Doherty, S. O.: Long-term trends in  
1188 ozone in baseline and European regionally-polluted air at Mace Head , Ireland over a 30-  
1189 year period, Atmos Environ, 179, 279–287, <https://doi.org/10.1016/j.atmosenv.2018.02.024>,  
1190 2018.

1191 [Derwent, R. G., Parrish, D. D., Manning, A. J., Spain, T. G., Simmonds, P. G., and O’Doherty,](#)  
1192 [S.: Ozone at Mace Head, Ireland from 1987 to 2021: Declining baselines, phase-out of](#)  
1193 [European regional pollution, COVID-19 impacts, Atmos Environ, 320,](#)  
1194 <https://doi.org/10.1016/j.atmosenv.2023.120322>, 2024.

Deleted: a

Deleted: Derwent, R. G., Manning, A. J., Simmonds, P. G., Spain, T. G., and O’Doherty, S.: Long-term trends in ozone in baseline and European regionally-polluted air at Mace Head, Ireland over a 30-year period, → Atmos → Environ, → 179, → 279–287, <https://doi.org/10.1016/j.atmosenv.2018.02.024>, 2018b.

1202 Ding, J., Dai, Q., Fan, W., Lu, M., Zhang, Y., Han, S., and Feng, Y.: Impacts of meteorology  
1203 and precursor emission change on O<sub>3</sub> variation in Tianjin, China from 2015 to 2021, J  
1204 Environ  
1205 Sci (China), 126, 506–516, <https://doi.org/10.1016/j.jes.2022.03.010>, 2023.  
1206 Donlon, B., Cahalane, A., and Fanning, A.: Ireland's State of the Environment Report 2024  
1207 Editors, 2024.

1208 Draxler, R. R. Evaluation of an Ensemble Dispersion Calculation.  
1209 <http://wesley.wwb.noaa.gov/reanalysis.html>,2003.

1210 EEA. Trends and projections in Europe 2024. <https://doi.org/10.2800/7574066,2024>.

1211 [Emmons, L. K., Hess, P. G., Lamarque, J.-F., and Pfister, G. G.: Tagged ozone mechanism for](#)  
1212 [MOZART-4, CAM-chem and other chemical transport models, Atmos. Chem. Phys., 12, 4607–](#)  
1213 [4622, . <https://doi.org/10.5194/acp-12-4607-2012,2012>.](#)

1214 [Finch, D. P., & Palmer, P. I., Increasing ambient surface ozone levels over the UK accompanied](#)  
1215 [by fewer extreme events. Atmospheric Environment, 237, 117627,](#)  
1216 <https://doi.org/https://doi.org/10.1016/j.atmosenv.2020.117627, 2020>.

1217

1218 Fiore, A. M., Dentener, F. J., Wild, O., Cuvelier, C., Schultz, M. G., Hess, P., Textor, C.,  
1219 Schulz,  
1220 M., Doherty, R. M., Horowitz, L. W., MacKenzie, I. A., Sanderson, M. G., Shindell, D. T.,  
1221 Stevenson, D. S., Szopa, S., Van Dingenen, R., Zeng, G., Atherton, C., Bergmann, D., Bey,  
1222 I.,  
1223 Carmichael, G., Collins, W. J., Duncan, B. N., Faluvegi, G., Folberth, G., Gauss, M., Gong,  
1224 S.,  
1225 Hauglustaine, D., Holloway, T., Isaksen, I. S. A., Jacob, D. J., Jonson, J. E., Kaminski, J. W.,  
1226 Keating, T. J., Lupu, A., Manner, E., Montanaro, V., Park, R. J., Pitari, G., Pringle, K. J., Pyle,

Formatted: Indent: Left: 0 cm, First line: 0 cm

1227 J. A., Schroeder, S., Vivanco, M. G., Wind, P., Wojcik, G., Wu, S., and Zuber, A.: Multimodel  
1228 estimates of intercontinental source-receptor relationships for ozone pollution, *Journal of*  
1229 *Geophysical Research Atmospheres*, 114, <https://doi.org/10.1029/2008JD010816>, 2009.

1230 Fowler, D., Coyle, M., Skiba, U., Sutton, M. A., Cape, J. N., Reis, S., Sheppard, L. J., Jenkins,  
1231 A., Grizzetti, B., Galloway, J. N., Vitousek, P., Leach, A., Bouwman, A. F., Butterbach-Bahl,  
1232 K., Dentener, F., Stevenson, D., Amann, M., and Voss, M.: The global nitrogen cycle in the  
1233 Twentyfirst century, *Philosophical Transactions of the Royal Society B: Biological Sciences*,  
1234 368, <https://doi.org/10.1098/rstb.2013.0164>, 2013.

1235 Girach, I. A., Tripathi, N., Nair, P. R., Sahu, L. K., and Ojha, N.: O<sub>3</sub> and CO in the South  
1236 Asian outflow over the Bay of Bengal: Impact of monsoonal dynamics and chemistry, *Atmos*  
1237 *Environ*, 233, <https://doi.org/10.1016/j.atmosenv.2020.117610>, 2020.

1238 Griffiths, P. T., Murray, L. T., Zeng, G., Shin, Y. M., Abraham, N. L., Archibald, A. T., Deushi,  
1239 M., Emmons, L. K., Galbally, I. E., Hassler, B., Horowitz, L. W., Keeble, J., Liu, J., Moeini,  
1240 O., Naik, V., and Connor, F. M. O.: Tropospheric ozone in CMIP6 simulations, 4187–4218,  
1241 2021.

1242 Grigas, T., Ovadnevaite, J., Ceburnis, D., Moran, E., McGovern, F. M., Jennings, S. G., and  
1243 O’Dowd, C.: Sophisticated Clean Air Strategies Required to Mitigate Against Particulate  
1244 Organic Pollution, *Sci Rep*, 7, <https://doi.org/10.1038/srep44737>, 2017.

1245 Guerreiro, C. B. B., Foltescu, V., and de Leeuw, F.: Air quality status and trends in Europe,  
1246 *Atmos Environ*, 98, 376–384, <https://doi.org/10.1016/j.atmosenv.2014.09.017>, 2014.

1247 [Huang, M., Carmichael, G. R., Pierce, R. B., Jo, D. S., Park, R. J., Flemming, J., Emmons, L.](#)  
1248 [K., Bowman, K. W., Henze, D. K., Davila, Y., Sudo, K., Jonson, J. E., Lund, M. T., Janssens-](#)  
1249 [Maenhout, G., Dentener, F. J., Keating, T. J., & Saiz-Lopez, A. \(2017\). Impact of](#)  
1250 [intercontinental pollution transport on North American ozone air pollution: An HTAP phase 2](#)

1251 [multi-model study. Atmospheric Chemistry and Physics, 17\(9\), 5721–5750.](#)

1252 <https://doi.org/10.5194/acp-17-5721-2017>

1253

Formatted: Indent: Left: 0 cm, First line: 0 cm

1254 IPCC, Masson-Delmotte, V., Zhai, P., Chen, Y., Goldfarb, L., Gomis, M. I., Matthews, J. B.  
1255 R., Berger, S., Huang, M., Yelekçi, O., Yu, R., Zhou, B., Lonnoy, E., Maycock, T. K.,  
1256 Waterfield, T., Leitzell, K., & Caud, N. Working Group I Contribution to the Sixth  
1257 Assessment Report of the Intergovernmental Panel on Climate Change Edited by.  
1258 www.ipcc.ch,2021.

1259 Jacobson, M. Z.: Atmospheric Pollution: History, Science, and Regulation, Cambridge  
1260 University Press, Cambridge, 2002.

1261 Jeon, W. B., Lee, S. H., Lee, H., Park, C., Kim, D. H., and Park, S. Y.: A study on high ozone  
1262 formation mechanism associated with change of NOx/VOCs ratio at a rural area in the  
1263 Korean Peninsula, Atmos Environ, 89, 10–21,  
1264 <https://doi.org/10.1016/j.atmosenv.2014.02.005>, 2014.

1265 Jonson, J. E., Stohl, A., Fiore, A. M., Hess, P., Szopa, S., Wild, O., Zeng, G., Dentener, F. J.,  
1266 Lupu, A., Schultz, M. G., Duncan, B. N., Sudo, K., Wind, P., Schulz, M., Marnmer, E.,  
1267 Cuvelier,  
1268 C., Keating, T., Zuber, A., Valdebenito, A., Dorokhov, V., De Backer, H., Davies, J., Chen,  
1269 G.

1270 H., Johnson, B., Tarasick, D. W., Stübi, R., Newchurch, M. J., Von Der Gathen, P.,  
1271 Steinbrecht, W., and Claude, H.: A multi-model analysis of vertical ozone profiles, Atmos  
1272 Chem Phys, 10,  
1273 5759–5783, <https://doi.org/10.5194/acp-10-5759-2010>, 2010.

1274 Khiem, M., Ooka, R., Huang, H., Hayami, H., Yoshikado, H., and Kawamoto, Y.: Analysis  
1275 of the Relationship between Changes in Meteorological Conditions and the Variation in

1276 Summer Ozone Levels over the Central Kanto Area, *Advances in Meteorology*, 2010, 1–13,  
1277 <https://doi.org/10.1155/2010/349248>, 2010.

1278 Lamarque, J. F. and Solomon, S.: Impact of changes in climate and halocarbons on recent  
1279 lower  
1280 stratosphere ozone and temperature trends, *J Clim*, 23, 2599–2611,  
1281 <https://doi.org/10.1175/2010JCLI3179.1>, 2010.

1282 Lamarque, J. F., Kinnison, D. E., Hess, P. G., and Vitt, F. M.: Simulated lower stratospheric  
1283 trends between 1970 and 2005: Identifying the role of climate and composition changes,  
1284 *Journal of Geophysical Research Atmospheres*, 113, <https://doi.org/10.1029/2007JD009277>,  
1285 2008.

1286 Lamarque, J. F., Bond, T. C., Eyring, V., Granier, C., Heil, A., Klimont, Z., Lee, D., Liousse,  
1287 C., Mieville, A., Owen, B., Schultz, M. G., Shindell, D., Smith, S. J., Stehfest, E., Van  
1288 Aardenne, J., Cooper, O. R., Kainuma, M., Mahowald, N., McConnell, J. R., Naik, V., Riahi,  
1289 K., and Van Vuuren, D. P.: Historical (1850-2000) gridded anthropogenic and biomass  
1290 burning emissions of reactive gases and aerosols: Methodology and application, *Atmos*  
1291 *Chem Phys*, 10, 7017–7039, <https://doi.org/10.5194/acp-10-7017-2010>, 2010.

1292 Lamarque, J. F., Emmons, L. K., Hess, P. G., Kinnison, D. E., Tilmes, S., Vitt, F., Heald, C.  
1293 L., Holland, E. A., Lauritzen, P. H., Neu, J., Orlando, J. J., Rasch, P. J., and Tyndall, G. K.:  
1294 CAMchem: Description and evaluation of interactive atmospheric chemistry in the  
1295 Community Earth  
1296 System Model, *Geosci Model Dev*, 5, 369–411, <https://doi.org/10.5194/gmd-5-369-2012>,  
1297 2012.

1298 Lefohn, A. S., Malley, C. S., Smith, L., Wells, B., Hazucha, M., Simon, H., Naik, V., Mills,  
1299 G.,

1300 Schultz, M. G., Paoletti, E., De Marco, A., Xu, X., Zhang, L., Wang, T., Neufeld, H. S.,  
1301 Musselman, R. C., Tarasick, D., Brauer, M., Feng, Z., Tang, H., Kobayashi, K., Sicard, P.,  
1302 Solberg, S., and Gerosa, G.: Tropospheric ozone assessment report: Global ozone metrics for  
1303 climate change, human health, and crop/ecosystem research, *Elementa*, 6,  
1304 <https://doi.org/10.1525/elementa.279>, 2018.

1305 Lin, M., Fiore, A. M., Cooper, O. R., Horowitz, L. W., Langford, A. O., Levy, H., Johnson,  
1306 B. J., Naik, V., Oltmans, S. J., and Senff, C. J.: Springtime high surface ozone events over  
1307 the western United States: Quantifying the role of stratospheric intrusions, *Journal of*  
1308 *Geophysical Research Atmospheres*, 117, <https://doi.org/10.1029/2012JD018151>, 2012.

1309 [Lin, Y., Jiang, F., Zhao, J., Zhu, G., He, X., Ma, X., Li, S., Sabel, C. E., and Wang, H.: Impacts](#)  
1310 [of O<sub>3</sub> on premature mortality and crop yield loss across China, \*Atmos. Environ.\*, \*\*194\*\*, 41–47,](#)  
1311 <https://doi.org/10.1016/j.atmosenv.2018.09.024>, 2018.

1312 Lupaşcu, A., Otero, N., Minkos, A., and Butler, T.: Attribution of surface ozone to NO<sub>x</sub> and  
1313 volatile organic compound sources during two different high ozone events, *Atmos Chem*  
1314 *Phys*, 22, 11675–11699, <https://doi.org/10.5194/acp-22-11675-2022>, 2022.

1315 [McVeigh, P., O'Dowd, C., and Berresheim, H.: Eddy Correlation Measurements of Ozone](#)  
1316 [Fluxes over Coastal Waters West of Ireland, \*Advances in Meteorology\*, 2010,](#)  
1317 <https://doi.org/10.1155/2010/754941>, 2010.

1318 Moiseenko, K. B., Vasileva, A. V., Skorokhod, A. I., Belikov, I. B., Repin, A. Y., and  
1319 Shtabkin,  
1320 Y. A.: Regional Impact of Ozone Precursor Emissions on NO<sub>x</sub> and O<sub>3</sub> Levels at ZOTTO  
1321 Tall Tower in Central Siberia, *Earth and Space Science*, 8,  
1322 <https://doi.org/10.1029/2021EA001762>, 2021.

Deleted: ¶

Deleted: Masson-Delmotte, V., Zhai, P., Chen, Y., Goldfarb, L., Gomis, M. I., Matthews, J. B. R., Berger, ¶ S., Huang, M., Yelekçi, O., Yu, R., Zhou, B., Lonnoy, E., Maycock, T. K., Waterfield, T., Leitzell, K., and Caud, N.: Working Group I Contribution to the Sixth Assessment Report of the Intergovernmental Panel on Climate Change Edited by, 2021. ¶

1331 Molod, A., Takacs, L., Suarez, M., and Bacmeister, J.: Development of the GEOS-5  
1332 atmospheric general circulation model: Evolution from MERRA to MERRA2, *Geosci Model*  
1333 *Dev*, 8, 1339–1356, <https://doi.org/10.5194/gmd-8-1339-2015>, 2015.

1334 Monks, P. S., Archibald, A. T., Colette, A., Cooper, O., Coyle, M., Derwent, R., Fowler, D.,  
1335 Granier, C., Law, K. S., Mills, G. E., Stevenson, D. S., Tarasova, O., Thouret, V., Von  
1336 Schneidmesser, E., Sommariva, R., Wild, O., and Williams, M. L.: Tropospheric ozone and  
1337 its precursors from the urban to the global scale from air quality to short-lived climate forcer,  
1338 <https://doi.org/10.5194/acp-15-8889-2015>, 13 August 2015.

1339 [Nalam, A., Lupascu, A., Ansari, T., and Butler, T.: Regional and sectoral contributions of NO<sub>x</sub>](#)  
1340 [and reactive carbon emission sources to global trends in tropospheric ozone during the 2000–](#)  
1341 [2018 period, \*Atmos. Chem. Phys.\*, 25, 5287–5311, <https://doi.org/10.5194/acp-25-5287-2025>,](#)  
1342 [2025.](#)

1343 [Nelson, B. S., et al.: Urban ozone trends in Europe and the USA \(2000–2021\), \*Atmos. Chem.\*](#)  
1344 [Phys., 25, 16009–16032, <https://doi.org/10.5194/acp-25-16009-2025>, 2025](#)

1345 O’Dowd, C., Ceburnis, D., Ovadnevaite, J., Vaishya, A., Rinaldi, M., and Facchini, M. C.:  
1346 Do anthropogenic, continental or coastal aerosol sources impact on a marine aerosol  
1347 signature at Mace Head?, *Atmos Chem Phys*, 14, 10687–10704, <https://doi.org/10.5194/acp->  
1348 [14-106872014](#), 2014.

1349 [Oltmans, S.J., Lefohn, A.S., Harris, J.M., Galbally, I., Scheel, H.E., Bodeker, G., Brunke, E.,](#)  
1350 [Claude, H., Tarasick, D., Johnson, B.J. and Simmonds, P.: Long-term changes in tropospheric](#)  
1351 [ozone. \*Atmos Environ\*, 40\(17\), 3156-3173, <https://doi.org/10.1016/j.atmosenv.2006.01.029> .](#)  
1352 [2006.](#)

1353 Oltmans, S. J., Lefohn, A. S., Shadwick, D., Harris, J. M., Scheel, H. E., Galbally, I., Tarasick,

**Deleted:** Nalam, A., Lupascu, A., Ansari, T., and Butler, T.: Regional and sectoral contributions of NO<sub>x</sub> and reactive carbon emission sources to global trends in tropospheric ozone during the 2000– 2018 period, <https://doi.org/10.5194/egusphere-2024-432>, 12 March 2024. ¶

**Formatted:** Indent: Left: 0.01 cm, Right: 0 cm, Line spacing: Double

1359 D. W., Johnson, B. J., Brunke, E. G., Claude, H., Zeng, G., Nichol, S., Schmidlin, F., Davies,  
1360 J., Cuevas, E., Redondas, A., Naoe, H., Nakano, T., and Kawasato, T.: Recent tropospheric  
1361 ozone changes - A pattern dominated by slow or no growth, *Atmos Environ*, 67, 331–351,  
1362 <https://doi.org/10.1016/j.atmosenv.2012.10.057>, 2013.

1363 [Ordóñez, C., Garrido-Perez, J. M., & García-Herrera, R. Early spring near-surface ozone in](#)  
1364 [Europe during the COVID-19 shutdown: Meteorological effects outweigh emission changes.](#)  
1365 [Science of The Total Environment, 747, 141322.](#)  
1366 <https://doi.org/https://doi.org/10.1016/j.scitotenv.2020.141322>, 2020.

1367 [Pallé, E., and Butler, C.J.: Comparison of sunshine records and synoptic cloud observations:](#)  
1368 [a case study for Ireland." \*Physics and Chemistry of the Earth, Parts A/B/C\* 27.6-8: 405-414,](#)  
1369 [2002.](#)

1370 [Pan, C., Zhu, B., Gao, J., Hou, X., Kang, H., and Wang, D.: Quantifying Arctic lower](#)  
1371 [stratospheric ozone sources in winter and spring, \*Sci Rep\*, 8,](#)  
1372 <https://doi.org/10.1038/s41598018-27045-5>, 2018.

1373 Paoletti, E.: Impact of ozone on Mediterranean forests: A review, *Environmental Pollution*,  
1374 144, 463–474, <https://doi.org/10.1016/j.envpol.2005.12.051>, 2006.

1375 Parrish, D. D., Derwent, R. G., Steinbrecht, W., Stübi, R., Van Malderen, R., Steinbacher, M.,  
1376 Trickl, T., Ries, L., & Xu, X.. Zonal Similarity of Long-Term Changes and Seasonal Cycles  
1377 of  
1378 Baseline Ozone at Northern Midlatitudes. *Journal of Geophysical Research: Atmospheres*,  
1379 125(13), 1–19. <https://doi.org/10.1029/2019JD031908>, 2020.

1380 Pausata, F. S. R., Pozzoli, L., Vignati, E., & Dentener, F. J.. North Atlantic Oscillation and  
1381 tropospheric ozone variability in Europe: Model analysis and measurements  
1382 intercomparison.

Deleted: ¶

Deleted: Pall E E, E. and Butler, C. J.: Comparison of sunshine records and synoptic cloud observations: a case study for Ireland, n.d. ¶

1387 Atmospheric Chemistry and Physics, 12(14), 6357–6376. <https://doi.org/10.5194/acp->  
1388 126357-2012,2012.

1389 Pio, C. A., Feliciano, M. S., Vermeulen, A. T., and Sousa, E. C.: Seasonal variability of ozone  
1390 dry deposition under southern European climate conditions, in Portugal, Atmospheric  
1391 Environment, 195–205 pp., 2000.

1392 Russo, M. R., Kerridge, B. J., Abraham, N. L., Keeble, J., Latter, B. G., Siddans, R., Weber,  
1393 J., Griffiths, P. T., Pyle, J. A., and Archibald, A. T.: Seasonal , interannual and decadal  
1394 variability of tropospheric ozone in the North Atlantic : comparison of UM-UKCA and  
1395 remote sensing observations for 2005 – 2018, 6169–6196, 2023.

1396 [Saiz-Lopez, A., Mahajan, A. S., Abbatt, J., Bobrowski, N., Brown, S. S., Burrows, J. P.,](#)  
1397 [Carpenter, L. J., Chipperfield, M. P., Cuevas, C. A., Fernandez, R., Hossaini, R., Kinnison,](#)  
1398 [D. E., Lamarque, J.-F., Finlayson-Pitts, B. J., Plane, J. M. C., Platt, U., Pratt, K., Ravishankara,](#)  
1399 [A. R., Salawitch, R. J., Saltzman, E. S., Simpson, W. R., Solomon, S., Thornton, J. A., & Wang,](#)  
1400 [T.: The influence of short-lived halogens on atmospheric chemistry and climate, Nature, 648,](#)  
1401 [289–299, https://doi.org/10.1038/s41586-025-09753-x, 2025.](#)

1402 [Seinfeld, J. H. and Pandis, S. N.: Atmospheric Chemistry and Physics: From Air Pollution to](#)  
1403 [Climate Change, 3rd edn., Wiley, Hoboken, NJ, 2016.](#)

1404 [Shindell, D. T., Chin, M., Dentener, F., Doherty, R. M., Faluvegi, G., Fiore, A. M., Hess, P.,](#)  
1405 Koch, D. M., Mackenzie, I. A., Sanderson, M. G., Schultz, M. G., Schulz, M., Stevenson, D.  
1406 S., Teich, H., Textor, C., Wild, O., Bergmann, D. J., Bey, I., Bian, H., Cuvelier, C., Duncan,  
1407 B.  
1408 N., Folberth, G., Horowitz, L. W., Jonson, J., Kaminski, J. W., Marmer, E., Park, R., Pringle,  
1409 K. J., Schroeder, S., Szopa, S., Takemura, T., Zeng, G., Keating, T. J., and Zuber, A.:  
1410 Atmospheric Chemistry and Physics A multi-model assessment of pollution transport to the  
1411 Arctic, Atmos. Chem. Phys, 5353–5372 pp., 2008.

Deleted: ¶

1413 Sicard, P., Serra, R., and Rossello, P.: Spatiotemporal trends in ground-level ozone  
1414 concentrations and metrics in France over the time period 1999-2012, *Environ Res*, 149,  
1415 122– 144, <https://doi.org/10.1016/j.envres.2016.05.014>, 2016.

1416 Simmonds, P. G., Derwent, R. G., Manning, A. L., and Spain, G.: Significant growth in  
1417 surface ozone at Mace Head, Ireland, 1987-2003, *Atmos Environ*,  
1418 38, 4769–4778, <https://doi.org/10.1016/j.atmosenv.2004.04.036>, 2004.

1419 Soares, J., UBA, D. P., UBA, S. K., EEA, A. G. O., EEA, A. G., & Horálek, J. Health Risk  
1420 Assessment of Air Pollution: assessing the environmental burden of disease in Europe in  
1421 2021. ETC HE Report, 7, 104, 2021.

1422 Spohn, T. K., Martin, D., Geever, M., and O'Dowd, C.: Effect of COVID-19 lockdown on  
1423 regional pollution in Ireland, *Air Qual Atmos Health*, 15, 221–234,  
1424 <https://doi.org/10.1007/s11869-021-01098-4>, 2022.

1425 [Stein, A. F., Draxler, R. R., Rolph, G. D., Stunder, B. J. B., Cohen, M. D., and Ngan, F.: NOAA's  
1426 HYSPLIT atmospheric transport and dispersion modeling system, \*Bulletin of the American  
1427 Meteorological Society\*, 96, 2059–2077, <https://doi.org/10.1175/BAMS-D-14-00110.1>, 2015.](#)

1428 Stunder, B.J.B.: Global Data Assimilation System (GDAS) Archive Information, NOAA Air  
1429 Resources Laboratory, Silver Spring, MD, USA, December 1, 2004

1430 [Sudo, K., and H. Akimoto, H.: Global source attribution of tropospheric ozone: Long-range  
1431 transport from various source regions, \*J. Geophys. Res.\*, 112, D12302,  
1432 \[doi:10.1029/2006JD007992\]\(https://doi.org/10.1029/2006JD007992\), 2007.](#)

1433 [Tan, J., Fu, J. S., Dentener, F., Sun, J., Emmons, L., Tilmes, S., Flemming, J., Takemura, T.,  
1434 Bian, H., Zhu, Q., Yang, C. E., and Keating, T.: Source contributions to sulfur and nitrogen  
1435 deposition - An HTAP II multi-model study on hemispheric transport, \*Atmos Chem Phys\*,  
1436 18, 12223–12240, <https://doi.org/10.5194/acp-18-12223-2018>, 2018.](#)

Formatted: Space After: 12.6 pt

Deleted: ¶

Deleted: ¶

Deleted: Seinfeld, J. H. and Pandis, S. N.: *Atmospheric Chemistry and Physics: From Air Pollution to Climate Change*, Wiley-VCH, New York, 1997. ¶  
Seinfeld, J. H. and Pandis, S. N.: *Atmospheric Chemistry and Physics: From Air Pollution to Climate Change*, 3rd edn., Wiley, Hoboken, NJ, 2016. ¶

Formatted: Font colour: Text 1

Formatted: Indent: Left: 0.01 cm, Right: 0 cm, Line spacing: Double

Deleted: Tafidis, P., Gholamnia, M., Sajadi, P., Krishnan Vijayakrishnan, S., and Pilla, F.: Evaluating the impact of urban traffic patterns on air pollution emissions in Dublin: a regression model using google project air view data and traffic data, *European Transport Research Review*, 16, <https://doi.org/10.1186/s12544-024-00671-z>, 2024. ¶

1451 Tavella, R. A. and da Silva Júnior, F. M. R.: Watch out for trends: did ozone increased or  
 1452 decreased during the COVID-19 pandemic?, *Environmental Science and Pollution Research*,  
 1453 28, 67880–67885, <https://doi.org/10.1007/s11356-021-17142-w>, 2021.

1454 Tilmes, S., Sanderson, B. M., and O'Neill, B. C.: Climate impacts of geoengineering in a  
 1455 delayed mitigation scenario, *Geophys Res Lett*, 43, 8222–8229,  
 1456 <https://doi.org/10.1002/2016GL070122>, 2016.

1457 Tilmes, S., Lamarque, J. F., Emmons, L. K., Kinnison, D. E., Ma, P. L., Liu, X., Ghan, S.,  
 1458 Bardeen, C., Arnold, S., Deeter, M., Vitt, F., Ryerson, T., Elkins, J. W., Moore, F., Spackman,  
 1459 J. R., and Val Martin, M.: Description and evaluation of tropospheric chemistry and aerosols  
 1460 in the Community Earth System Model (CESM1.2), *Geosci Model Dev*, 8, 1395–1426,  
 1461 <https://doi.org/10.5194/gmd-8-1395-2015>, 2015.

1462 Todorović, M. N., Radenković, M. B., Rajšić, S. F., & Ignjatović, L. M. Evaluation of  
 1463 mortality attributed to air pollution in the three most populated cities in Serbia. *International*  
 1464 *Journal of Environmental Science and Technology*, 16(11), 7059–7070.  
 1465 <https://doi.org/10.1007/s13762019-02384-6>, 2019.

1466 Tripathi, O. P., Jennings, S. G., O'Dowd, C. D., Coleman, L., Leinert, S., O'Leary, B., Moran,  
 1467 E., O'Doherty, S. J., and Spain, T. G.: Statistical analysis of eight surface ozone measurement  
 1468 series for various sites in Ireland, *Journal of Geophysical Research Atmospheres*, 115, 1–20,  
 1469 <https://doi.org/10.1029/2010JD014040>, 2010.

1470 Tripathi, O. P., Jennings, S. G., O'Dowd, C., O'Leary, B., Lambkin, K., Moran, E.,  
 1471 O'Doherty, S. J., and Gerard Spain, T.: An assessment of the surface ozone trend in Ireland  
 1472 relevant to air pollution and environmental protection, *Atmos Pollut Res*, 3,  
 1473 341–351, <https://doi.org/10.5094/APR.2012.038>, 2012.

Formatted: Space After: 0 pt, Line spacing: Multiple 1.99 li

Deleted: ¶

Deleted: →

Deleted: →

Deleted: →

Deleted: →

Deleted:

Deleted: →

Deleted: →

Deleted: ¶

1482 Tripathi, O. P., Jennings, S. G., Colman, L., Lambkin, K., Moran, E., and Dowd, C. O.: Ozone  
1483 levels , changes and trends over Ireland – an Integrated Analysis, 2013.

1484 Tripathi, O. P., Gerard Jennings, S., Colman, L., Lambkin, K., and Moran, E.: EPA STRIVE  
1485 Programme 2007-2013 Ozone levels, changes and trends over Ireland-an Integrated Analysis  
1486 (2006-AQ-MS-50) STRIVE Report, n.d.

1487 Tripathi, R. M., Vinod Kumar, A., Manikandan, S. T., Bhalke, S., Mahadevan, T. N., and  
1488 Puranik, V. D.: Vertical distribution of atmospheric trace metals and their sources at Mumbai,  
1489 India, *Atmos Environ*, 38, 135–146, <https://doi.org/10.1016/j.atmosenv.2003.09.006>, 2004.

1490 Vautard, R., Moran, M. D., Solazzo, E., Gilliam, R. C., Matthias, V., Bianconi, R., Chemel,  
1491 C.,  
1492 Ferreira, J., Geyer, B., Hansen, A. B., Jericevic, A., Prank, M., Segers, A., Silver, J. D.,  
1493 Werhahn, J., Wolke, R., Rao, S. T., and Galmarini, S.: Evaluation of the meteorological  
1494 forcing used for the Air Quality Model Evaluation International Initiative (AQMEII) air  
1495 quality simulations, *Atmos Environ*, 53, 15–37,  
1496 <https://doi.org/10.1016/j.atmosenv.2011.10.065>, 2012.

1497 [Van Der Werf, G. R., Randerson, J. T., Giglio, L., Collatz, G. J., Mu, M., Kasibhatla, P. S.,](#)  
1498 [Morton, D. C., Defries, R. S., Jin, Y., and Van Leeuwen, T. T.: Global fire emissions and the](#)  
1499 [contribution of deforestation, savanna, forest, agricultural, and peat fires \(1997-2009\), \*Atmos\*](#)  
1500 [Chem Phys](#), 10, 11707–11735, <https://doi.org/10.5194/acp-10-11707-2010>, 2010.

1501 [Wespes, C., Hurtmans, D., Clerbaux, C., and Coheur, P. F.: O3 variability in the troposphere](#)  
1502 [as observed by IASI over 2008-2016: Contribution of atmospheric chemistry and dynamics,](#)  
1503 [J Geophys Res](#), 122, 2429–2451, <https://doi.org/10.1002/2016JD025875>, 2017.

1504 WHO. Global Air Quality Guidelines: Particulate Matter (PM2.5 and PM10), Ozone,  
1505 Nitrogen Dioxide, Sulfur Dioxide and Carbon Monoxide (World Health Organization, 2021).

**Deleted:** Van Der Werf, G. R., Randerson, J. T., Giglio, L., Collatz, G. J., Mu, M., Kasibhatla, P. S., Morton, D. C., Defries, R. S., Jin, Y., and Van Leeuwen, T. T.: Global fire emissions and the contribution of deforestation, savanna, forest, agricultural, and peat fires (1997-2009), *Atmos Chem Phys*, 10, 11707–11735, <https://doi.org/10.5194/acp-10-11707-2010>, 2010.

1513 [Wild, O. & Ryan, E. M.: Quantifying and addressing the uncertainties in tropospheric ozone](#)  
1514 [and OH in a global chemistry transport model, EGU sphere \[preprint\],](#)  
1515 <https://doi.org/10.5194/egusphere-2025-4534>, 2025.

1516 [Yan, Y., et al.: Analysis of European ozone trends in the period 1995–2014, Atmos. Chem.](#)  
1517 [Phys., 18, 5589–5605, https://doi.org/10.5194/acp-18-5589-2018](#), 2018.

1518 Yerramilli, A., Srinivas Challa, V., Rao Dodla, V. B., Myles, L. T., Pendergrass, W. R., Vogel,  
1519 C. A., Tului, F., Baham, J. M., Hughes, R., Patrick, C., Young, J., & Swanier, S. Simulation  
1520 of surface ozone pollution in the Central Gulf Coast region during summer synoptic condition  
1521 using WRF/Chem air quality model. Atmospheric Pollution Research, 3(1), 55–71.  
1522 <https://doi.org/10.5094/APR.2012.005>, 2012.

1523 Young, P. J., Archibald, A. T., Bowman, K. W., Lamarque, J., Naik, V., Stevenson, D. S., and  
1524 Tilmes, S.: Pre-industrial to end 21st century projections of tropospheric ozone from the  
1525 Atmospheric Chemistry and Climate Model Intercomparison Project ( ACCMIP ), 2063–  
1526 2090, <https://doi.org/10.5194/acp-13-2063-2013>, 2013.

1527 [Yu, H., Chin, M., West, J. J., Atherton, C. S., Bellouin, N., Bergmann, D., Bey, I., Bian, H.,](#)  
1528 [Diehl, T., Forberich, O., Hess, P., Schulz, M., Takemura, T., & Tan, Q. A multimodel](#)  
1529 [assessment of the influence of regional anthropogenic emission reductions on aerosol direct](#)  
1530 [radiative forcing and the role of intercontinental transport. Journal of Geophysical Research:](#)  
1531 [Atmospheres, 118\(13\), 7004–7025. https://doi.org/10.1002/jgrd.50502](#), 2013.

1532  
1533 Zhang, J. J., Wei, Y., & Fang, Z. Ozone pollution: A major health hazard worldwide. Frontiers  
1534 in Immunology, 10(OCT), 1–10. <https://doi.org/10.3389/fimmu.2019.02518>, 2019.

Formatted: Indent: Left: 0.01 cm, First line: 0 cm, Right: 0 cm, Line spacing: Double

Formatted: Underline, Font colour: Custom Colour (RGB(238,0,0))

Formatted: Indent: Left: 0 cm, First line: 0 cm

Formatted: Indent: Left: 0.01 cm

1535 [Zhang, C. and Stevenson, D.: Characteristic changes of ozone and its precursors in London](#)  
1536 [during COVID-19 lockdown and the ozone surge reason analysis. Atmos. Environ., 273,](#)  
1537 [118980, https://doi.org/10.1016/j.atmosenv.2022.118980,2022](https://doi.org/10.1016/j.atmosenv.2022.118980,2022)

Formatted: Indent: Left: 0.01 cm, Right: 0 cm, Line spacing: Double

1538 Zhu, T., Melamed, M., Parrish, D., Gauss, M., Klenner, L. G., Lawrence, M., Konare, A., and  
1539 Lioussé, C.: Impacts of Megacities on Air Pollution and Climate, WMO, Geneva, 2012.

Formatted: Font colour: Text 1

1540

1541

1542

1543

1544

#### 1545 **Figure Captions**

1546 **Figure 1.** The map of EPA O<sub>3</sub> measurement sites over Ireland with classification of  
1547 backgrounds.

1548 **Figure 2.** Annual average O<sub>3</sub> concentration at different sites in Ireland. In each box, the  
1549 lowest whisker level represents the 5<sup>th</sup> percentile, the box spans from the 25<sup>th</sup> to the 75<sup>th</sup>  
1550 percentile, the horizontal line within the box represents the median 50<sup>th</sup> percentile, and the  
1551 upper whisker represents the 95<sup>th</sup> percentile. The average of monthly O<sub>3</sub> values calculated  
1552 for the entire period of each station, and the red line shows the average monthly O<sub>3</sub>  
1553 variation of all sites top axis shows the month (1– 12).

1554 **Figure 3.** Monthly trend analysis of O<sub>3</sub> at different sites for 10 year period. (2012-2022)  
1555 Adopting the trend reliability scale defined for TOAR-II studies (Chang et al., 2023), trends  
1556 with very high certainty are marked by \*\*\*( $p \leq 0.001$ ), , trends with high certainty with

1557 **\*\***( $p \leq 0.01$ ), and low to medium certainty with **\*\***( $p \leq 0.05$ ). Positive trends are in red  
1558 shade and negative trends are in blue shade.

1559 **Figure 5.-** Trend in O<sub>3</sub> precursors NO<sub>2</sub> (a), and CH<sub>4</sub> (b) at different sites. Trends with very  
1560 high certainty are marked by **\*\*\***( $p \leq 0.001$ ), trends with high certainty with **\*\***( $p \leq$   
1561  $0.01$ ), and low to medium certainty with **\***( $p \leq 0.05$ ).

1562 **Figure 6.** Percentage change in NO<sub>2</sub> and O<sub>3</sub> during the lockdown period of 2020 as  
1563 compared to the 2017-2019 average at different sites in Ireland for (a) March (b) April  
1564 (c) May Month.

1565 **Figure 7.** The comparison of Monthly CAM4 – Chem O<sub>3</sub> and Monthly O<sub>3</sub> observations at  
1566 five sites in Ireland.

1567 **Figure 8.** Absolute contribution of major NO<sub>x</sub> sources (a) (NO<sub>x</sub> Tagging) and VOC  
1568 source (b) (NO<sub>x</sub> Tagging) to the CAM4-Chem simulated surface O<sub>3</sub> for the Mace Head grid  
1569 cell between 2000-2018.

1570 **Figure 9.** Trends in contributions to monthly average modelled Mace Head grid cell surface  
1571 O<sub>3</sub> at for the 2000-2018 period derived from (a) NO<sub>x</sub> tagging and (b) VOC tagging.

1572 **Figure 10.** Trend in seasonal Average of observed O<sub>3</sub> (black) and Model O<sub>3</sub> (red) at Mace  
1573 head, separated into clean sector and EU-influenced sector.

1574 **Figure 11.** Exceedances measured at Mace Head per month from 2000 until 2022, during  
1575 the clean air sector (green) and EU influenced sector (yellow). The percentage of both to  
1576 total exceedances is shown in the inlay.

1577 **Figure 12.** (a) The trend in Spring-time exceedances measured at Mace Head between  
1578 2000 and 2022 (blue) with the clean-air exceedances (gold), and (b) The trend in 95th

1579 percentile of spring (Mar- May) O<sub>3</sub> measured in µg /m<sup>3</sup> for the clean sector (blue) and the  
1580 EUinfluenced sector (gold).

1581 **Figure 13** Monthly cumulative Mace Head grid cell O<sub>3</sub> contributions to EU influenced  
1582 sector and clean sector exceedances (a) NO<sub>x</sub> tagging and (b) VOC tagging Mace Head grid  
1583 cell.

1584

1585

1586

1587

1588

<b>Page 7: [1] Deleted</b>	<b>Coleman, Liz</b>	<b>30/01/2026 13:37:00</b>
----------------------------	---------------------	----------------------------



<b>Page 16: [2] Deleted</b>	<b>Coleman, Liz</b>	<b>30/01/2026 16:12:00</b>
-----------------------------	---------------------	----------------------------



<b>Page 29: [3] Deleted</b>	<b>Coleman, Liz</b>	<b>30/01/2026 16:49:00</b>
-----------------------------	---------------------	----------------------------

